Fall 2009

On the generation of isotopic disequilibrium during crustal anatexis of ancient metasedimentary and granitic rocks

Julie Elizabeth Barkman
University of New Hampshire, Durham

ON THE GENERATION OF ISOTOPIC DISEQUILIBRIUM DURING CRUSTAL ANATEXIS OF ANCIENT METASEDIMENTARY AND GRANITIC ROCKS

BY

JULIE ELIZABETH BARKMAN

B.A., Boston University, 2007

THESIS

Submitted to the University of New Hampshire

in Partial Fulfillment of

the Requirements for the Degree of

Master of Science

in

Earth Sciences: Geology

September, 2009

This thesis has been examined and approved.

Thesis Director, Julia G. Bryce, Assistant Professor of Geochemistry

Jo Laird, Associate Professor of Earth Sciences

Ethan F. Baxter, Associate Professor of Earth Sciences, Boston University

August 14, 2009

Date

DEDICATION

This work is dedicated to my mom, who has always been what I hope to be when I grow up.

ACKNOWLEDGEMENTS

I would like to thank my advisor, Julie Bryce, for all of her help and the long hours she has spent with me on this work. I would also like to thank Ethan Baxter, who has guided and supported me since I was doing my undergraduate work at Boston University. Additionally, I want to thank Jo Laird for her amazing petrological skills and ability to identify almost any mineral known to mankind in thin section.

Thank you to all of the staff at Rensselaer Polytechnic Institute for all of your assistance and for making me feel welcome in your lab. I would especially like to thank Bruce Watson for allowing me to visit and use his equipment. Additionally, I would like to thank Jay Thomas for all of his help and guidance in running my experiments.

I would also like to thank the UNH Department of Earth Sciences for providing me with a TA fellowship, the TESSE program for supporting me with a graduate fellowship, and the National Science Foundation for their Graduate Research Fellowship that will continue to support me during my Ph.D.

Lastly, I would like to thank my family and friends for all of their support during my graduate studies. Without your encouragement I don't think I could have accomplished all that I have.

TABLE OF CONTENTS

DEDICATION iii

ACKNOWLEDGEMENTS iv

LIST OF TABLES vii

LIST OF FIGURES viii

ABSTRACT x

CHAPTER PAGE

1. INTRODUCTION 1

    1.1. Nature of Crustal Melting 4

    1.2. Project Overview 5

2. MODELING ISOTOPIC DISEQUILIBRIUM DURING PARTIAL MELTING 7

    2.1. Previous Partial Melt Studies 7

        2.1.1. Prior Experimental Work 7

        2.1.2. Existing Partial Melting Models 8

        2.1.3. Implications and Remaining Questions 10

    2.2. Partial Melting Model 12

        2.2.1. Model Parameters 12

        2.2.2. Case Studies 16

    2.3. Limitations of Theoretical Approach 26

3. INFLUENCE OF SOURCE COMPOSITION ON MELT CHEMISTRY 28

    3.1. MELTS Modeling 28

3.2. Effect of Protolith Age 33

3.3. Role of Accessory Phases 36

3.3.1. Apatite and Monazite 37

3.3.2. Zircon 39

3.4. Influence of Water 41

4. PRELIMINARY EXPERIMENTS 42

4.1. Sample Information 42

4.2. Mineralogical and Petrographic Description 44

4.3. Experiment Setup and Design 47

4.5. Melt Generation and Rock Texture 51

5. IMPLICATIONS OF ISOTOPIC DISEQUILIBRIUM 52

5.1. Assimilation of Partial Melts into Basalts 52

5.1.1. Limitations of Traditional Assimilation Models 53

5.1.2. Bulk Rock versus Partial Melt Contamination 54

5.2. Diffusive Re-equilibration in Residual Phases 57

6. CONCLUSIONS AND APPLICATIONS 62

LIST OF REFERENCES 63

APPENDIX 73

LIST OF TABLES

TABLE	PAGE
1. Mineralogy of model rock compositions	16
2. Composition of basalt and components assimilating	55
A1. U, Th, and Pb compositions of individual minerals	73
A2. Rb, Sr, Sm, and Nd compositions of individual minerals	74
A3. Unmodified whole rock compositions from other studies	74
A4. Experimental run products	75
A5. Experimental melt compositions	76
A6. Calculated trace element concentrations of whole rocks	77
A7. Trace element concentrations of partial melts	78
A8. Zircon solubility data	85
A9. Major element composition of Antler Granite	85
A10. Trace element composition of Antler Granite	86

LIST OF FIGURES

FIGURE	PAGE
1. (A) Cartoon of migmatization	3
1. (B) Cartoon of assimilation	3
2. Isotopic disequilibrium in Sr	5
3. Sr isotopic evolution in schist	8
4. Isotopic disequilibrium of composition MP	19
5. Accessory phases in residual for composition MP	20
6. Isotopic disequilibrium of composition MS	22
7. Accessory phases in residual for composition MS	23
8. Isotopic disequilibrium of composition MW	25
9. Accessory phases in residual for composition MW	26
10. pHMELTS vs experiments: Melt fraction of SMAG	32
11. pHMELTS vs experiments: Melt compositions of SMAG	32
12. Isotopic evolution of Sr over time	34
13. Effect of age on isotopic disequilibrium	35
14. Apatite dissolution in melt	38
15. Zircon dissolution in melt	40
16. Geologic map of Hualapai Mountains	43
17. (A) Zircon and apatite in thin section	45
17. (B) Apatite included in biotite in thin section	45
18. (A) Zircon along a grain boundary in thin section	46
18. (B) Myrmekite in thin section	46

19. Piston cylinder sample capsule 49

20. (A) BSE image of mica breaking down 50

20. (B) BSE image of experimentally generated melt 50

21. $^{87}Sr/^{86}Sr$ vs ε_{Nd} of whole rock and melts assimilating 56

22. $^{206}Pb/^{204}Pb$ vs $^{208}Pb/^{204}Pb$ of whole rock and melts assimilating 57

23. Diffusive re-equilibration of Nd and Pb in apatite 61

A1. Trace element concentrations of melts from composition MP 79

A2. Trace element concentrations of melts from composition MS 80

A3. Trace element concentrations of melts from composition MW 81

A4. pHMELTS vs experiments: Melt fraction of MS 82

A5. pHMELTS vs experiments: Melt fraction of MW 82

A6. pHMELTS vs experiments: Melt compositions of MS 83

A7. pHMELTS vs experiments: Melt compositions of MW 84

ABSTRACT

ON THE GENERATION OF ISOTOPIC DISEQUILIBRIUM DURING CRUSTAL ANATEXIS OF ANCIENT METASEDIMENTARY AND GRANITIC ROCKS

by

Julie Elizabeth Barkman

University of New Hampshire, September, 2009

Partial melting of rocks may lead to the generation of melts in isotopic disequilibrium with their source rocks. To examine the amount of disequilibrium created during anatexis in the Sr, Nd, and Pb isotopic systems, a model was producing using results of partial melt experiments to constrain the breakdown of major minerals during melting. Experimentally derived mineral dissolution equations were employed to account for contributions from accessory phases. Based upon results from this study, partial melts, especially from ancient rocks, are likely to be in considerable disequilibrium. The behavior of important accessory minerals during anatexis appears to exert considerable control over the magnitude of disequilibrium. The results of this work may have important implications for models of mass transfer during magmatism and for reconstructing temperature-time scales during episodes of crustal heating.

CHAPTER 1

INTRODUCTION

The chemical composition of a rock can reveal the complex history of its origins and evolution through time. Elemental and isotopic characteristics of magma bodies are used as a way to comprehend the processes relevant to their formation. For metamorphic rocks, they can provide information on the timing and duration of periods of deformation and metasomatism, as well as the original age of the rock sample. In regions where rapid crustal heating or high-grade metamorphism occur, crustal anatexis, or the partial melting of rock, can be influential on rock chemistry. The elemental and isotopic compositions of melts generated during anatexis have been employed to answer a variety of geologic questions, from identifying sources of plutonic bodies (e.g. Himalayan leucogranites, Harris *et al.* 1995 and Patiño Douce & Harris 1998, or the Goat Ranch pluton, Zeng *et al.* 2005(a)) to establishing rates of crustal growth (e.g. Jacobsen 1988). Furthermore, the chemical consequences of partial melting are used to gain insight into magma chamber processes such as assimilation (e.g. DePaolo 1981).

Accordingly, the isotopic consequences of anatexis are especially important to understand the processes of migmatization and assimilation (Fig. 1). Migmatites form as the result of prograde metamorphism advancing to the point where rocks

partially melt (Fig. 1(A)). The exposure to significant amounts of heat and pressure causes minerals with lower melting points and/or greater solubilities to melt out forming leucosomes (felsic partial melts in migmatites) and melanosomes (mafic residual material), leaving behind the parent rock, known as the mesosome (Wimmenauer & Bryhni 2007). Because accessory phases can dictate melt composition, it is essential to ascertain how isotopes and trace elements partition between the mesosome, melanosome, and leucosome in order to understand the influence of these minerals. The accessibility of migmatites makes them a valuable field-based counterpart through which assumptions can be tested about partial melts formed deeper in Earth's crust.

When magma travels through continental crust it can partially melt and assimilate the surrounding wallrock, thereby inheriting some of the elemental and isotopic signature of the melt (Fig. 1(B)). This process creates complicated magma compositions because they not only reflect their source but also the crustal input; the incorporation of partial melt is said to "contaminate" the geochemical signature of the magma (Knesel & Davidson 1996). Additionally, the chemistry of continental magmas can be affected by several other processes, including mantle source mixing and fractional crystallization occurring in the crust during its transport to the surface of the Earth. Full characterization of these processes is critical to improving our understanding of the origins of continental magmas; while several quantitative models satisfactorily account for some trace element and isotopic effects (DePaolo 1981, Spera & Bohrson 2001), all of them consider the isotopic composition of the assimilant to be the same as that of the

bulk rock. In particular, the influence of minor and accessory phases on magma chemistry is particularly poorly quantified, and therefore need to be properly constrained in order to better understand the relative significance of varying magma sources versus overprinting by processes in the magma chamber.

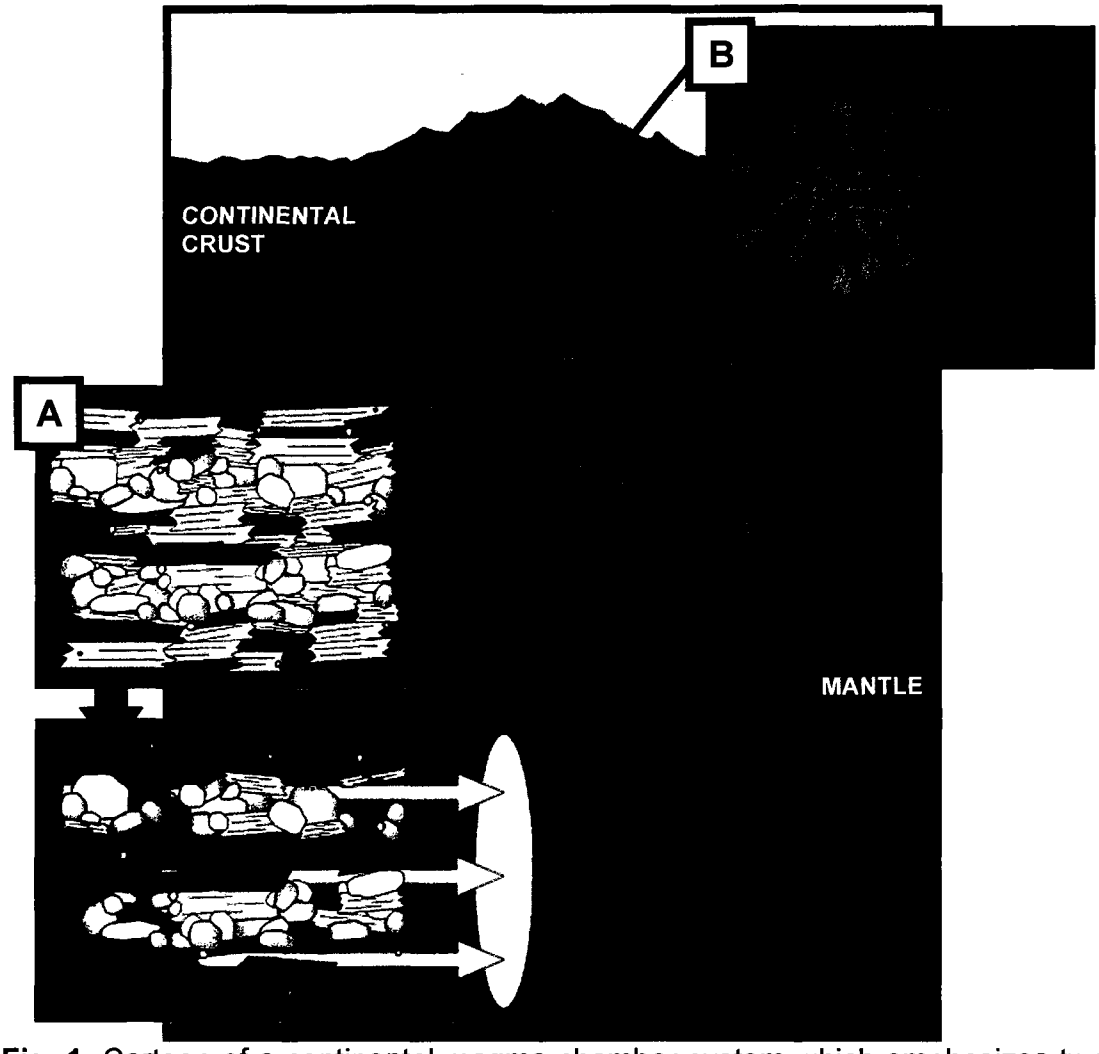

Fig. 1. Cartoon of a continental magma chamber system which emphasizes two processes that may potentially be affected by isotopic disequilibrium during crustal anatexis (Modified from Waters *et al.* 2004 and Kent *et al.* 2002). **(A)** Continental crust can partially melt producing granitic bodies from its melt and granulites from the residual material. If the melt generated is trapped in the source rock, then migmatites may form. **(B)** As magma ascends through the crust it can partially melt and assimilate some of the wallrock it travels through, incorporating some of the crustal geochemical signature into the magma.

1.1. Nature of Crustal Melting

The notion that the chemical compositions of partial melts are typically identical to that of the whole rocks producing them has been increasingly challenged (Watson & Harrison 1984, Hogan & Sinha 1991, Watt & Harley 1993, Bea 1996, Bea & Montero 1999, and others). Instead, it has become more widely accepted that crustal rocks often partially melt nonmodally, or certain minerals preferentially melt, due to differences in mineral solubilities (e.g. Le Breton & Thompson 1988, Gardien *et al.* 1995, Harris *et al.* 1995). Melts generated from this process bear trace element and isotopic signatures distinctive from their source rocks and are, accordingly, said to be in isotopic disequilibrium (Fig. 2, Knesel & Davidson 2002). Minor and accessory phase minerals often dominate trace element budgets and have extreme parent/daughter isotopic ratios. As such, they are able to exhibit great control over the chemistry of partial melts and magmas they may assimilate into. This influence extends over the isotopic and elemental systems most used for reconstructing the origin and movement of melts in the crust (namely lead, Pb, strontium, Sr, and neodymium, Nd). Additionally, it has been shown that the diffusion of these elements is slow, coefficients are typically $<10^{-16}$ cm^2/s (Brady 1995), compared to mineral dissolution rates which generally exceed 10^{-16} cm/s (Davies & Tommasini 2000). Consequently, in medium- to coarse-grained rocks (1-10mm grain size) where diffusional length scales are smaller than grain sizes, the Sr, Pb, and Nd isotopic systems can take several tens of millions of years to equilibrate and partial melts produced to remain in disequilibrium (Davies &

Tommasini 2000). Furthermore, even under petrographic conditions favoring isotopic equilibration, rapid melt extraction (on the order of thousands of years) may still prevent the system from doing so (e.g. Sawyer 1991, Ayres *et al.* 1996, Watt *et al.* 1996). The high probability of melts to be disequilibrium requires a greater understanding of the isotopic systems affected in order to make accurate geologic interpretations.

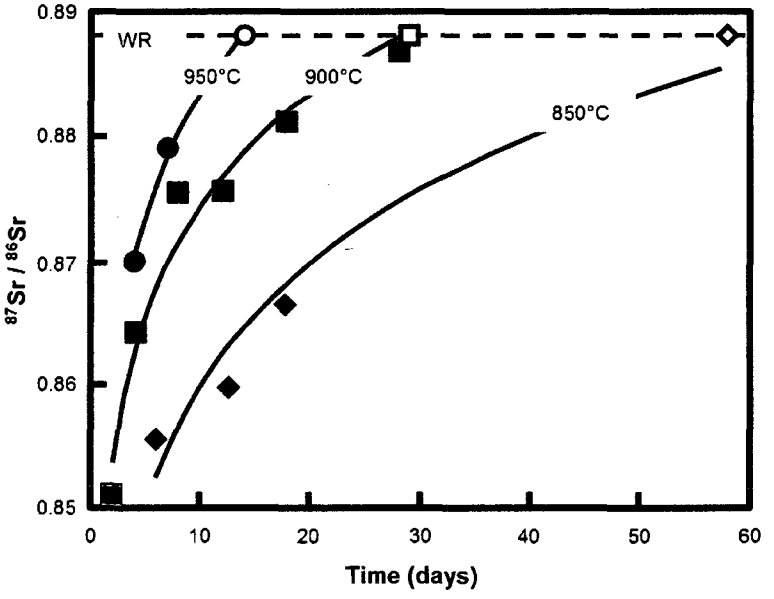

Fig. 2. $^{87}Sr/^{86}Sr$ ratios of partial melts from a Proterozoic biotite granite (Marble Mountains, California) at 850°C, 900°C, and 950°C achieve equilibrium with their whole rock over time; consequently, they may not be able to fully equilibrate with their source rock if they are rapidly removed (Fig. 1., Knesel & Davidson 2002).

1.2. Project Overview

The goal of this project was to examine isotopic disequilibrium during dehydration partial melting through theoretical and experimental means. A geochemical model was created to predict the influence of partial melting on the Sr, Nd, and Pb isotopic systems. This model combines mineral solubility

equations and partial melt experiments to determine phases entering the melt and the resulting isotopic composition. Chapter 2 outlines the parameters of the model as well as the results of several case studies examined. In Chapter 3 the pHMELTS thermodynamic algorithm was used to model the melting of rocks to enter into the partial melt model (Ghiorso & Sack 1995, Asimow & Ghiorso 1998, Smith & Asimow 2005). This chapter also discusses the major influences on melt isotopic composition, including the effects of age and important accessory phases. In Chapter 4 petrographic and preliminary observations of experimentally melted are employed to understand textual relationships between source rocks and melting. The geologic implications of disequilibrium melts are described in Chapter 5, and finally the conclusions of this study are presented in Chapter 6.

CHAPTER 2

MODELING ISOTOPIC DISEQUILIBRIUM DURING PARTIAL MELTING

2.1. Previous Partial Melt Studies

2.1.1. Prior Experimental Work

Several experimental studies have been conducted towards understanding the relationship between parent rock composition and the associated partial melts (Watt & Harley 1993, Hammouda *et al.* 1996, Knesel & Davidson 1996, Tommasini & Davies 1997, Patiño Douce & Harris 1998, Knesel & Davidson 1999, Knesel & Davidson 2002). Most have focused on the Sr isotopic system, particularly on the prominent role of mica in the elemental and isotopic budgets of melts. A partial melt experiment using a plagioclase and Sr-doped fluorphlogopite rock demonstrated that the Sr isotopic and elemental content of melts do not reflect the bulk assemblage (Hammouda *et al.* 1996). As shown in Fig. 3, mica can add a significant amount of Sr at the onset of melting due to the nonmodal nature of partial melting (Zeng *et al.* 2005(b)). Furthermore, Knesel & Davidson (2002) illustrated that large amounts of isotopic disequilibrium can be created with only small degrees of melting (Fig. 2). Over a range of temperatures melts approach equilibrium with the $^{87}Sr/^{86}Sr$ ratio of the whole rock; however, because melts may be removed as quickly as 2m/yr, over short

time scales they may not equilibrate with their sources prior to extraction (Knesel & Davidson 2002).

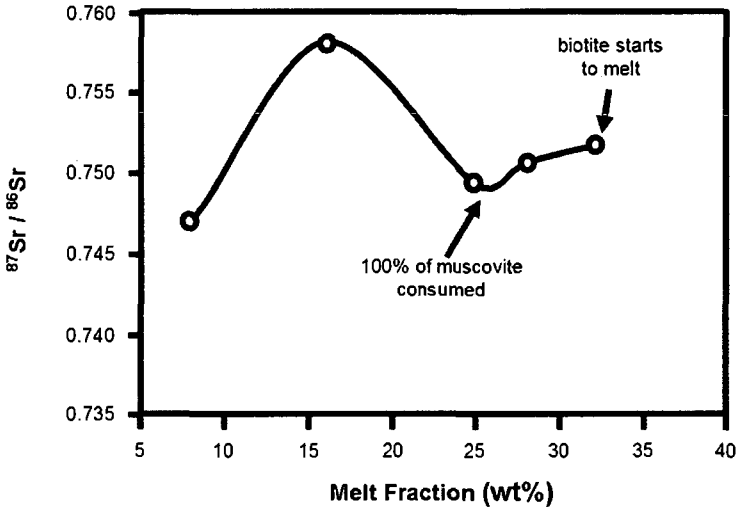

Fig. 3. Theoretical isotopic evolution of Sr in a partial melt due to dehydration melting of a High Himalayan Crystalline Sequence (HHCS) muscovite schist (modeled by Zeng *et al.* 2005(b) based upon experimental data collected by Patiño Douce & Harris 1998). The $^{87}Sr/^{86}Sr$ ratio of the partial melt is elevated during low degrees of melting when muscovite dehydration melting dominates and wanes as muscovite is consumed. The Sr isotopic signature then increases again with larger melt fractions as biotite starts to enter into the melt. $^{87}Sr/^{86}Sr$ of the whole rock prior to melting was 0.7417.

2.1.2. Existing Partial Melting Models

The partial melt model adapted in by Zeng *et al.* (2005(a)) builds upon the experimental framework for Sr and uses theoretical parameters to incorporate the Nd isotopic system. Melt composition and mineral modal abundances in the source rock and residual were based upon experimental data from the Patiño Douce & Harris (1998) study on dehydration melting of muscovite schist. Key accessory phases not involved in major mineral breakdown reactions were integrated into the model through experimentally derived mineral solubility

equations (Harrison & Watson 1984, Pichavant *et al.* 1992, Montel 1993). Elemental and isotopic compositions of partial melts were calculated based upon equations modeling trace element behavior in partial melts (see Section 2.2.1., Eq. 3-6, Allègre & Minister 1978, Prinzhofer & Allègre 1985, Barbey *et al.* 1989, Sawyer 1991).

Several existing experimental studies provide preliminary insights into the relative significance of mineral breakdown reactions on the parent-daughter isotopic systems (e.g. Knesel & Davidson 2002). The breakdown of minerals dominating the Rb-Sr system (namely muscovite, biotite, plagioclase, and potassium feldspar) is controlled by dehydration or water-fluxed melting reactions (Eq. 9 & 10, described in Patiño Douce & Harris (1998)). Conversely, accessory phases, holding large concentrations of rare earth elements (REE), can have the strongest influence on the Sm-Nd isotopic system. Of particular concern to Nd are apatite and monazite and, therefore, dissolution equations for both are included in the Zeng *et al.* (2005(a)) model (Harrison & Watson 1984, Montel 1993 respectively). While the main control on the solubility of these phases is temperature, apatite also exerts some influence over the dissolution of monazite. Their mutual structural component, phosphorus (P), causes these minerals to have competing effects during melting. Apatite's structure contains a larger percentage of P (~43 wt% P_2O_5 versus ~29 wt% P_2O_5 in monazite) and is also typically an order of magnitude more abundant than monazite in metapelites (Zeng *et al.* 2005(a)). Consequently, the solubility of monazite is highly dependent upon the dissolution of apatite, although other parameters such as

water content and melt composition are also significant (see Montel (1993) for complete parameterization). The solubility of monazite increases with higher water content, making its dissolution favored during low temperature, wet melting; apatite will remain mostly in the residual under these conditions. However, high temperature, dry melting favors apatite entering the melt; monazite dissolution is suppressed by the increasing concentration of phosphorus and LREE (light REE) in the melt. Because during low degrees of melting both phases do not typically go into the melt under the same water and temperature conditions, Zeng *et al.* (2005(a)) consider their dissolutions individually rather than synchronously.

The Zeng *et al.* (2005(a)) model is primarily important because of the contributions it makes to understanding the behavior of the Nd isotopic system during partial melting. The relationship between apatite and monazite dissolution and the influence it can have on the Nd isotopic composition of partial melts are explored. It also provides a theoretical basis for examining the isotopic effects of partial melting on Sr. The geochemical model created in this study expands upon the model adapted by Zeng *et al.* (2005(a)) by adding the Pb isotopic system into it.

2.1.3. Implications and Remaining Questions

Previous studies demonstrate that isotopic disequilibrium results from minor and accessory phase minerals, rather than major rock-forming phases, dictating the distribution of isotopes and trace elements between partial melts and source

rocks (Watt & Harley 1993, Bea 1996, Bea & Montero 1999, Knesel & Davidson 1999, Zeng *et al.* 2005(b), Zeng *et al.* 2005(c)). The Rb-Sr isotopic system is controlled mostly by muscovite, biotite, and mica breakdown reactions (Hammouda *et al.* 1996, Knesel & Davidson 1996, Tommasini & Davies 1997, Knesel & Davidson 1999, Knesel & Davidson 2002), while the Sm-Nd system is mostly influenced by the dissolution of apatite and monazite (Watson & Capobianco 1981, Rapp & Watson 1986, Zeng *et al.* 2005(a), Zeng *et al.* 2005(b), Zeng *et al.* 2005(c)). Furthermore, partial melt research thus far indicates that isotopic disequilibrium is likely a feature typical of crustal melts and as such assimilation models should be adjusted to reflect it (Hammouda *et al.* 1996, Knesel & Davidson 1996, Tommasini *et al.* 1997).

Despite the advances that have been made, there are still many unanswered questions about the implications of partial melts. Nd has been examined theoretically with Sr, as outlined in Section 2.2.2., but no experiments have been conducted to corroborate their findings (Zeng *et al.* 2005(a)). Pb has also not been studied experimentally; Hogan and Sinha (1991) modeled the effects of partial melting on Pb, but Sr and Nd are not included in their model for comparison. Evaluating all three isotopic systems simultaneously is valuable because each re-equilibrates under different conditions and timescales; establishing the decoupling of these systems may be useful for modeling conditions of lower crustal melts. Experimentally derived and analyzed melts are also important because models only generate the composition of partial melts that have not been allowed to re-equilibrate at all. While models are

advantageous because they are more inclusive of different rock compositions, experiments are critical to ground-truth theoretical findings and assess competing effects of mineral solubilities. Accordingly, both theoretical and experimental studies investigating the influence of partial melting on the Sr, Nd, and Pb isotopic systems and the consequences of assimilating these melts are needed.

2.2. Partial Melting Model

2.2.1. Model Parameters

In this study, a partial melting model based upon that adapted by Zeng *et al.* (2005(a)) was developed and utilized in order to examine the effects on the Sr, Nd, and Pb isotopic systems during dehydration melting. Several input parameters are amassed from published literature; including mineral trace element concentrations, source rock mineral modes, melt compositions, and residual mineral modes. U, Th, Pb, Rb, Sr, Sm, and Nd concentrations in each mineral comprising the rock melting were collected from trace element studies (see Appendix, Tables A1 and A2). When possible, concentrations were taken from the phases in metapelitic or granite rocks; where data were lacking, values from other rock types were used. Partial melt data were taken from several studies where initial rock, melt, and residual compositions are all reported. All this information is required in order to calculate the isotopic disequilibrium created due to partial melting; the mineral modes are needed to determine what major and minor phases are contributing to the melt, while the melt composition is necessary for calculating the input from accessory phases.

While major and minor mineral abundances entering the melt can be compiled from partial melt studies examining melting reactions, accessory phase contributions have to be modeled using solubility equations. As discussed in Section 2.1.2, dry and high temperature melting favors apatite entering the melt over monazite. This study focuses on dehydration melting and consequently only the dissolution of apatite was examined. Apatite dissolution is based on the partitioning of phosphorus between apatite and melt, which is dependent upon the temperature of melting and the silica (SiO_2) content of the melt (Harrison & Watson 1984):

$$\ln D_P^{Ap/Melt} = \frac{8400 + [10^4 \times 2.64(SiO_2 - 0.5)]}{T} - \{3.1 + [12.4 \times (SiO_2 - 0.5)]\} \quad \textbf{(1)}$$

where D is the partition coefficient of P between apatite and the melt, SiO_2 is the weight percent of silica in the melt, and T is the temperature in Kelvin. This solubility equation is applicable for compositions with 45-75% SiO_2 and 0-10% water and for the range of pressures and temperatures seen in the crust.

Zircon was also added as an accessory phase to modeled compositions but like apatite is not involved in the melting reaction. Accordingly, an experimentally determined solubility equation was used to approximate the amount of zircon entering into the melt (Watson & Harrison 1983):

$$\ln D_{Zr}^{Zircon/Melt} = \{-3.8 - [0.85(M-1)]\} + \frac{12900}{T} \quad \textbf{(2)}$$

where D is the partition coefficient of zirconium (Zr) between zircon and the melt, M is the cation ratio (Na + K + 2Ca)/(Al·Si) in the melt, and T is the temperature in Kelvin. This equation is calibrated for granitic crustal anatectic melts forming

at temperatures from 860°C up to 1500°C, where M = 0.9 to 1.7. Pressure and water content are not considered to be significant factors in determining zircon solubility and are excluded from the equation (Watson & Harrison 1983). The compositions of experimentally derived melts and the temperatures at which they were produced are used to determine the amount of both zircon and apatite entering the melt under those conditions.

Isotopic compositions were calculated for all minerals using the respective age equation for each isotopic system (see Appendix, Tables A1 and A2). Initial isotopic ratios for Sr, Pb, and Nd were set based upon ratios measured in ~1.7 Ga granitic composition rocks from (Lanphere 1969, Chamberlain & Bowring 2000, and Nelson and DePaolo 1985, respectively). The model also allows for other ages to be examined, however, 1.7 Ga was chosen because it is both geologically old and the age of a rock of experimental interest (this sample is discussed in Chapter 4 and was used for all preliminary experiments).

Trace element concentrations and isotopic compositions of the whole rock (WR) and partial melts were calculated using the following equations (Allègre & Minster 1978, Prinzhofer & Allègre 1985, Barbey *et al.* 1989, Sawyer 1991, Zeng *et al.* 2005(a)).

Trace element concentration of partial melt:

$$C_L^i = (x_{m1}C_1^i + x_{m2}C_2^i + \ldots x_{mn}C_n^i) - (y_{c1}c_1^i + y_{c2}c_2^i + \ldots y_{cn}c_n^i) \qquad \textbf{(3)}$$

$C_L^i =$ *concentration of element i in melt*

$x_{mj} =$ *weight proportion of mineral j entering melt*

y_{ck} = *weight proportion of mineral k crystallizing from melt*

C_j^i = *concentration of element i in mineral j*

c_k^i = *concentration of element i in mineral k*

Isotopic composition of partial melt (ε_{Nd} shown):

$$(\varepsilon_{Nd})_L = \frac{\sum x_{mi} C_{Nd}^i \varepsilon_{\mathrm{Nd}}^{\mathrm{mi}}}{\sum x_{mi} C_{Nd}^i} \quad \textbf{(4)}$$

$(\varepsilon_{Nd})_L$ = *Nd isotopic composition of melt*

ε_{Nd}^i = *Nd isotopic composition of mineral i*

Initial trace element concentration of source rock:

$$C_0^i = X_1 C_1^i + X_2 C_2^i + \ldots X_n C_n^i \quad \textbf{(5)}$$

C_0^i = *initial concentration of element i in source rock*

X_j = *weight proportion of mineral j in source*

Isotopic composition of source rock (ε_{Nd} shown):

$$(\varepsilon_{Nd})_{WR} = \frac{\sum X_{mi} C_{Nd}^i \varepsilon_{\mathrm{Nd}}^{\mathrm{mi}}}{\sum X_{mi} C_{Nd}^i} \quad \textbf{(6)}$$

$(\varepsilon_{Nd})_{WR}$ = *Nd isotopic composition of source rock*

Equation (4), which calculates the isotopic composition of the partial melts, assumes that each mineral entering the melt is able to preserve its Sr, Nd, and Pb isotopic composition. Example equations are given for the Nd isotopic system; Sr and Pb can be calculated using corresponding equations.

2.2.2. Case Studies

Source compositions and associated partial melt data from experimental studies were used as input parameters into the model created (Table 1, see Appendix, Tables A3-A5 for residual, melt, and unmodified source rock compositions). To investigate the isotopic disequilibrium created by dehydration melting mica-rich compositions were chosen; these types of rocks are commonly found in the crust and also typically contain minor and accessory minerals which dominate U-Th-Pb, Rb-Sr, and Sm-Nd budgets. The amount of disequilibrium predicted to occur by the model during partial melting of each source rock used is shown in Fig. 4, 6, and 8; disequilibrium is expressed as the difference between the isotopic ratio of the whole rock (WR) and the partial melt, where a value of zero indicates that the melt has equilibrated with the source.

Rock Sample	Mineral (weight percent)									
	Qtz	Pl	Ms	Bt	Grt	Als	Ilm	Apt	Mnz	Zrn
Metapelite (MP) [1]	31.00	4.00	10.00	29.74	5.00	19.00	1.00	0.25	---	0.01
Muscovite Schist (MS) [2]	43.00	28.00	22.00	2.00	4.50	---	---	0.50	0.01	---
Metagraywacke (MW) [3]	34.30	26.50	---	36.70	---	---	2.00	0.50	---	0.01

Table 1. Mineralogy of model rock compositions. Original compositions were modified in order to include accessory phases important to trace element budgets (biotite was lowered for MP and MW, garnet was lowered for MS). Qtz = quartz, Pl = plagioclase, Ms = muscovite, Bt = biotite, Grt = garnet, Als = aluminosilicate, Apt = apatite, Mnz = monazite, Ilm = ilmenite, Zrn = zircon ([1]Patiño Douce & Johnston 1991, [2]Patiño Douce & Harris 1998, [3]Patiño Douce & Beard 1996).

In each experimental study the rocks were partially melted under dry conditions, allowing for dehydration melting to proceed due to the breakdown of micas (Thompson 1982, Le Breton & Thompson 1988, Patiño Douce & Harris

1998, and others describe these reactions in detail). Compositions MP and MW have little or no muscovite, and consequently are controlled by similar melting reactions (Patiño Douce & Johnston 1991, Patiño Douce & Beard 1996, respectively):

$$\textbf{MP:}\quad Bt + Pl + Als + Qtz \rightarrow Melt + Grt \qquad (7)$$

$$\textbf{MW:}\quad Bt + Pl + Qtz \rightarrow Melt + Grt + Oxides \qquad (8)$$

Conversely, composition MS is controlled by the breakdown of muscovite (Patiño Douce & Johnston 1991):

$$\textbf{MS:}\quad Ms + Pl + Qtz \rightarrow Melt + Als \qquad (9)$$

Partial melt data for the MP composition were available for 18-60% melting at 10kbar, 825-1000°C (Appendix, Table A4). Amongst the three compositions examined MP shows the greatest disequilibrium for all isotopic ratios (Fig. 4), with the exception of the $^{208}Pb/^{204}Pb$ disequilibrium generated by composition MS (Fig. 6). As indicated by the arrows in Fig. 4, Sr is dominantly controlled by the micas; because all of the muscovite is consumed before 18% melting, biotite is particularly important in this case study. As melting proceeds biotite enters into the melt, and the $^{87}Sr/^{86}Sr$ ratio evolves towards that of the whole rock. Due to the large amount of biotite in the rock (Table 1), which contains significant amounts of radiogenic Sr, the melt products at 58% and 60% melting have $^{87}Sr/^{86}Sr$ ratios greater than that of the whole rock. The same trend in $^{87}Sr/^{86}Sr$ was observed in partial melts from a biotite granite analyzed by Knesel and Davidson (2002). The Pb isotopic system for this composition was most strongly influenced by garnet, apatite, and zircon. Of the minerals contained in this

sample, garnet has the most Th, which decays to ^{208}Pb, than every phase except zircon and apatite. As a result, when 1% of the garnet enters into the melt at 18% melting (as reported by Patiño Douce & Johnston 1991), a smaller amount of disequilibrium is seen for the $^{208}Pb/^{204}Pb$ ratio (Fig. 4); at all stages of melting thereafter garnet was, instead, observed to crystallizing from the melt. The $^{208}Pb/^{204}Pb$ ratio then remains in considerable disequilibrium, trending very slowly towards equilibrium, due to apatite and zircon residing predominantly in the residual material (as shown by Fig. 5). While these accessory phases do enter into the melt, they do so very slowly; by 60% melting less than 1.25% of the apatite and 0.5% of the zircon have left the source (Fig. 5). Consequently, a sizeable disequilibrium for both $^{206}Pb/^{204}Pb$ and $^{143}Nd/^{144}Nd$ is also maintained over the course of partial melting examined. While both apatite and zircon contribute to the disequilibrium seen in Pb, apatite, containing high concentrations of Nd, is primarily responsible for that seen in the $^{143}Nd/^{144}Nd$ ratios. This composition was modeled with (filled circles, Fig, 4) and without (open circles) the presence of zircon; because noticeable shifts were only seen for $^{208}Pb/^{204}Pb$ and $^{206}Pb/^{204}Pb$, this difference was not shown graphically for $^{87}Sr/^{86}Sr$ and $^{143}Nd/^{144}Nd$. The inclusion of just 0.01% zircon caused an increase in disequilibrium of approximately 0.7 for $^{206}Pb/^{204}Pb$. Less variance was seen in the disequilibrium generated for $^{208}Pb/^{204}Pb$ because the composition of zircon that was chosen was more U- than Th-rich.

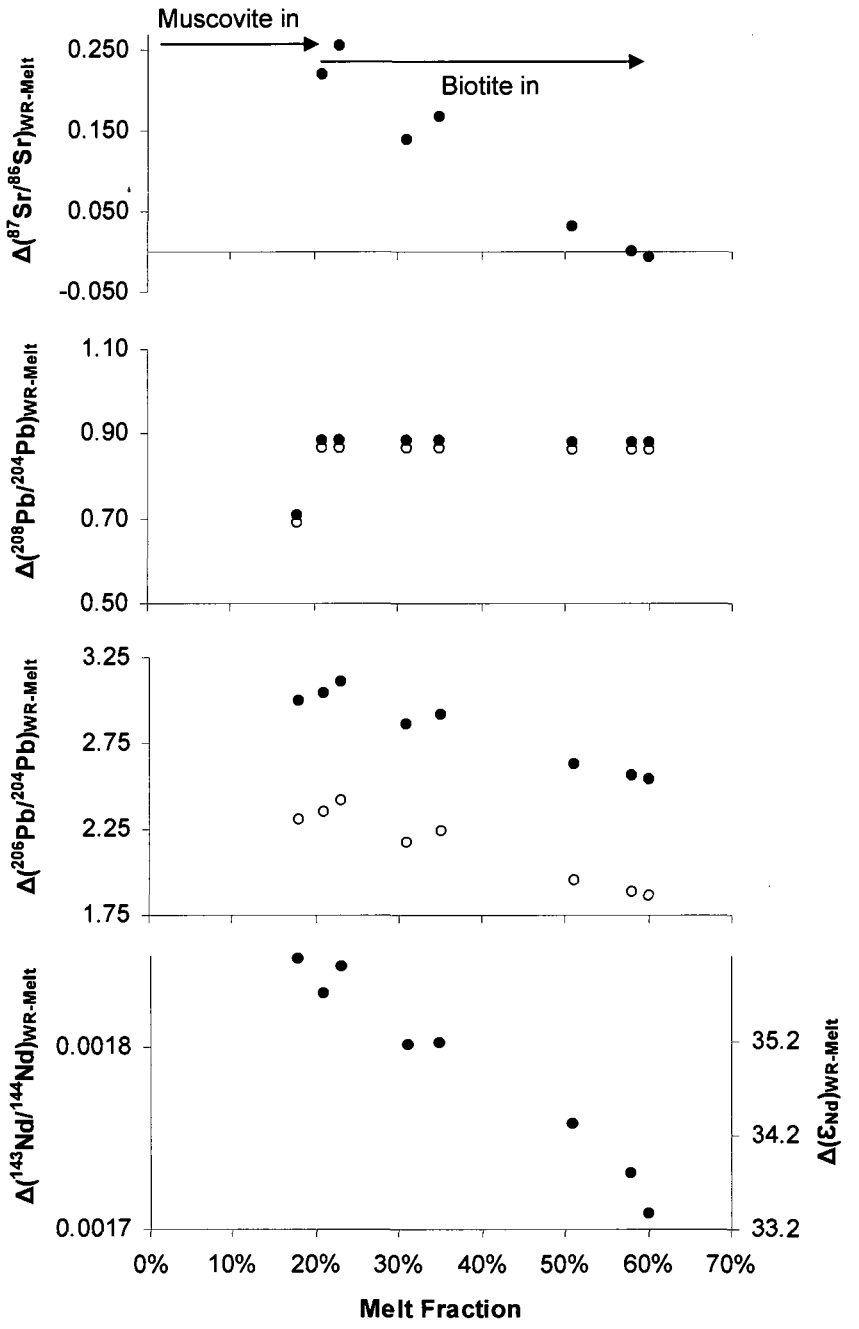

Fig. 4. Isotopic disequilibrium associated with composition MP when the age of the rock is set to 1.7 Ga. Disequilibrium is expressed as the difference between the isotopic ratio of the whole rock (WR) and the partial melt.

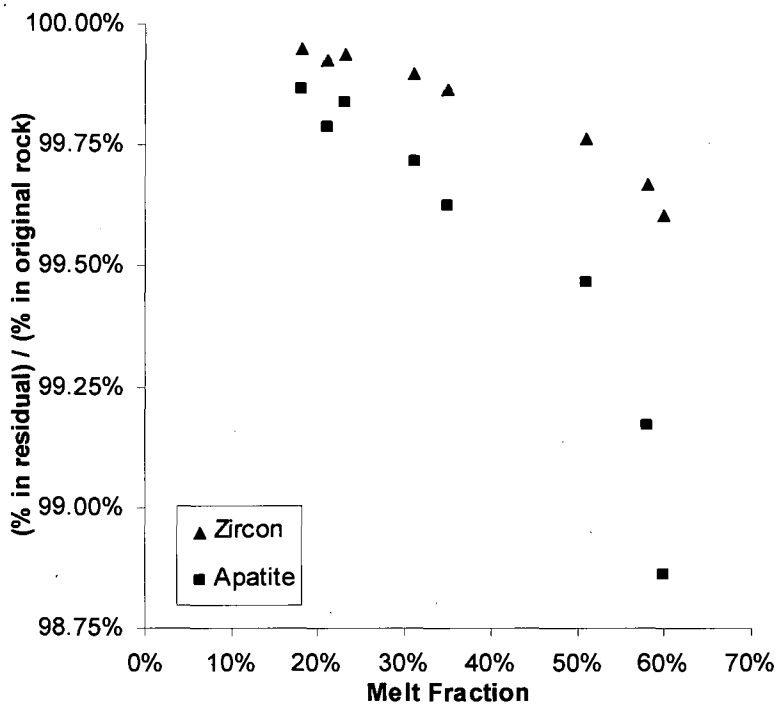

Fig. 5. Percentage of zircon and apatite staying in the residue during partial melting of composition MP.

Unlike the other compositions, partial melt data for rock sample MS were only available for 8-32% melting from 775-900°C at 6kbar (Appendix, Table A4); consequently, the isotopic systems do not trend back towards equilibrium as satisfactorily as MP and MW where data were collected for up to 60% melting. As discussed above, the progression of melting in this sample is controlled by muscovite (Eq. 9), which is exhausted after 25% melting allowing biotite dehydration melting to take over. Unlike the other two compositions, monazite was included as an accessory phase instead of zircon. Due to these two factors, the isotopic evolution of melts from this sample is more complicated. From 8% to 25% melting, the amount of disequilibrium for Sr increases and then decreases. As denoted by the arrows in Fig. 6, this trend is the result of muscovite being

completely consumed by 25% melting whereupon biotite breakdown takes over. The dips observed in Pb and Nd trends in Fig. 6 are linked with a 1.5% drop in SiO_2 content in the 16% partial melt, which directly influences the amount of apatite that is able to dissolve. The disequilibrium in $^{208}Pb/^{204}Pb$ is considerably greater than that seen in melts from rocks MP and MW because it contains monazite, which contains several orders of magnitude more Th than any other phase present (tens of ppm or less compared to several thousand ppm). As discussed in Section 2.1.2., during dry melting the dissolution of apatite dominates and forces monazite to remain in the residual. The sequestration of monazite in the residual combined with the slow dissolution rate of apatite allows for a large disequilibrium to be preserved in the $^{208}Pb/^{204}Pb$ ratio of the melt over significant degrees of melting. Monazite also contains extremely high concentrations of U, Pb, Sm, and Nd and consequently it also contributes significantly to the disequilibrium seen in $^{206}Pb/^{204}Pb$ and $^{143}Nd/^{144}Nd$ ratios. Furthermore, less than 1.5% of the apatite enters into the melt, adding to the $^{206}Pb/^{204}Pb$ and $^{143}Nd/^{144}Nd$ disequilibrium (Fig. 7).

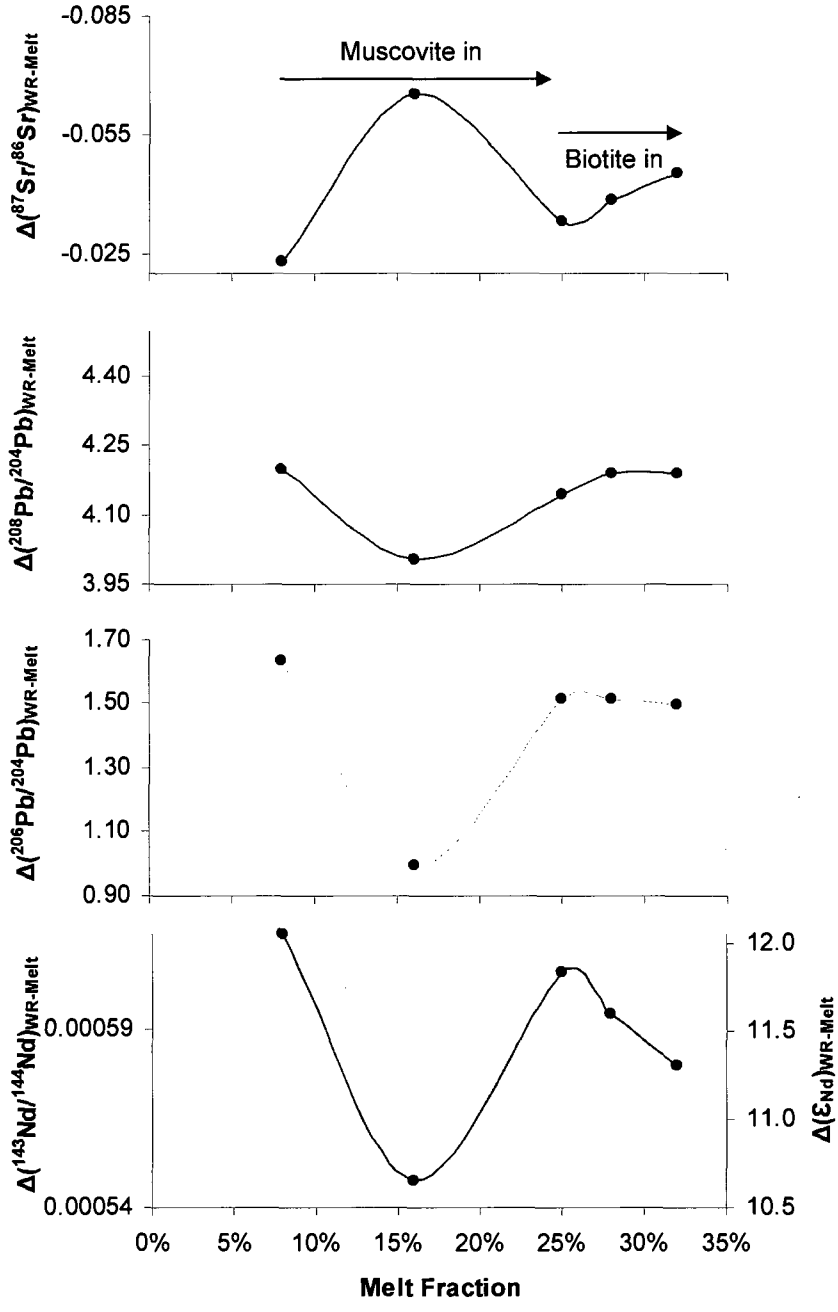

Fig. 6. Isotopic disequilibrium associated with composition MS when the age of the rock is set to 1.7 Ga. Disequilibrium is expressed as the difference between the isotopic ratio of the whole rock (WR) and the partial melt.

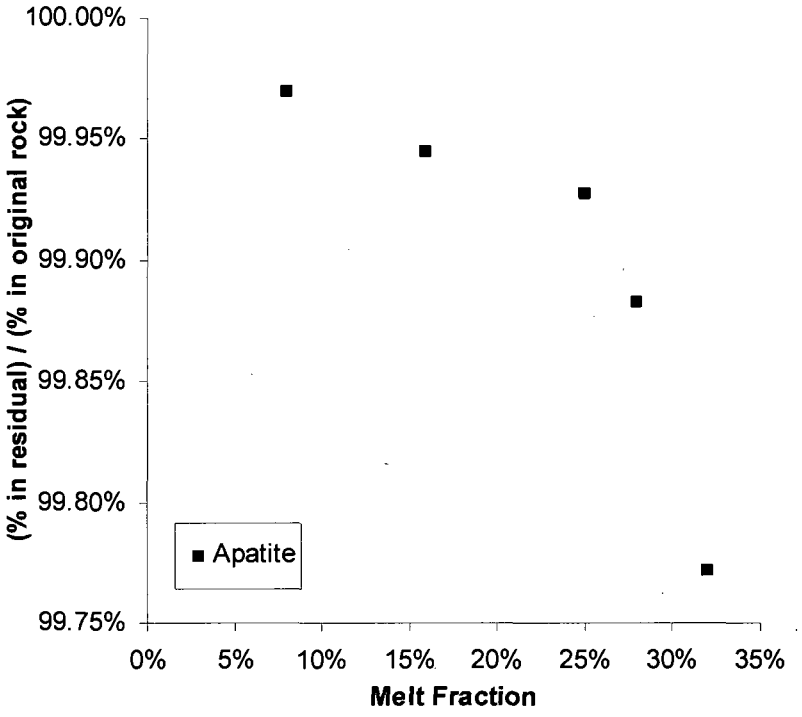

Fig. 7. Percentage of zircon and apatite staying in the residue during partial melting of composition MS.

For the last composition, MW, data were available for 26-60% melting for 850-950°C at 10kbar (Appendix, Table A4). As biotite enters into the melt (shown by the arrow in Fig. 8), $^{87}Sr/^{86}Sr$ trends back towards equilibrium; the slight shift in this trend seen from 56% to 60% melting results from the re-emergence of biotite reported by Patiño Douce and Beard (1996). This reappearance of biotite likely results from slight variations in whole rock compositions used in each experiment, heterogeneities in the grains of biotite themselves, or imprecision associated with estimating melt abundance. Like with sample MP, MW was modeled with and without zircon in order to see the magnitude of disequilibrium associated with it (filled and open circles used again and only shown for Pb, Fig.

8). The addition of 0.01% zircon causes an increase in the disequilibrium for both $^{208}Pb/^{204}Pb$ and $^{206}Pb/^{204}Pb$, although on a smaller scale than was observed in MP (Fig. 8). Less disequilibrium is seen for $^{208}Pb/^{204}Pb$ than in the other two compositions; this is attributed to the lack of a Th-rich phase, besides apatite which is found in the same abundance in all compositions, entering into the melt. As illustrated in Fig. 9, zircon and apatite are staying primarily in the residue, preventing Pb and Nd in the melt from reaching equilibrium.

The evolution of Sr, Pb, and Nd concentrations between the residual and the melt were also calculated; exact values determined can be found in Table A6 and A7 and Fig. A1-A3 in the Appendix. Each composition showed concentrations increasing in the melt as they decreased in the residual, although Nd was the only trace element examined where the concentration in the melt never exceeded that in the residual. Regardless of the melting reaction occurring or the accessory phases present, considerable disequilibrium between the whole rock and melt composition was created from small degrees of melting.

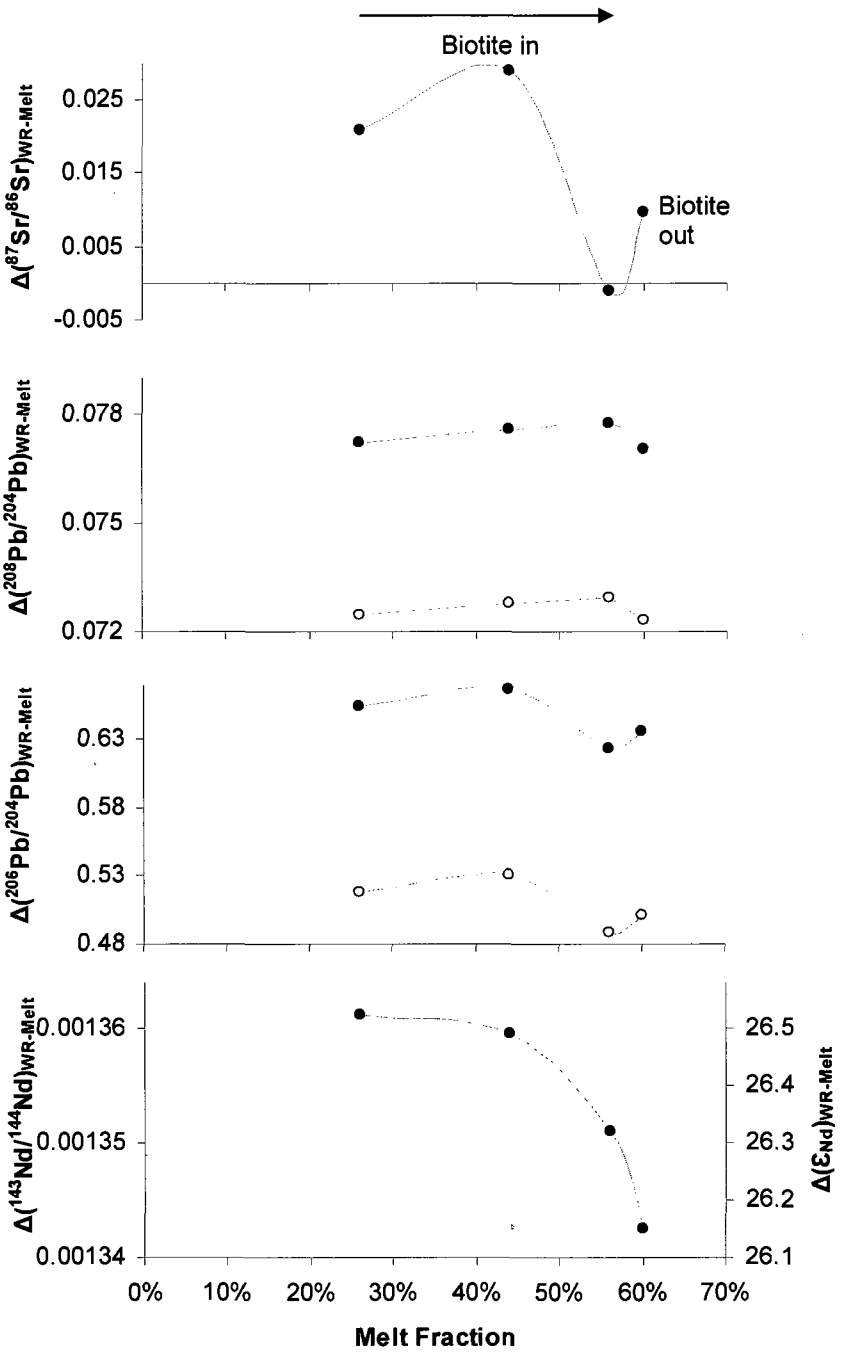

Fig. 8. Isotopic disequilibrium associated with composition MW when the age of the rock is set to 1.7 Ga. Disequilibrium is expressed as the difference between the isotopic ratio of the whole rock (WR) and the partial melt.

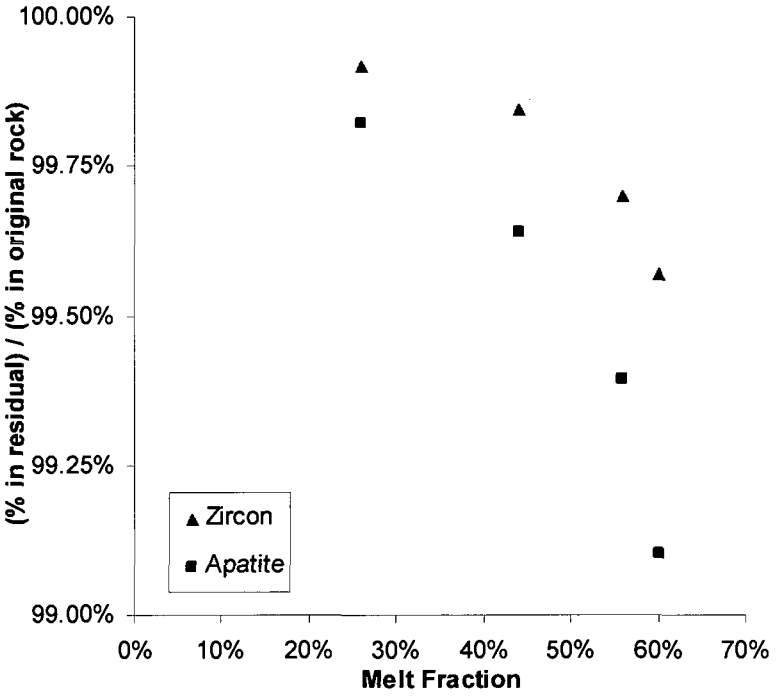

Fig. 9. Percentage of zircon and apatite staying in the residue during partial melting of composition MW.

2.3. Limitations of Theoretical Approach

While examining partial melting through modeling is beneficial in that it allows for a wide array of compositions to be researched, there are limitations to this methodology. Accessory phases pose a significant problem because they play a substantial role in trace element budgets but are not involved in melting reactions and therefore have to be accounted for with solubility equations. Consequently, minerals which do not have experimentally derived dissolution equations must necessarily be excluded. Even with these equations, however, each type of mineral is looked at individually. In cases where the solubility of one or more phases influences that of others, such as monazite and apatite, this may prove to be an inadequate treatment. Additionally, the use of mineral dissolution

equations restricts the compositions that can be modeled to those which have been experimentally established.

An additional obstacle with theoretical studies is that they require a certain amount of knowledge about the rock melting and its partial melt products. The model developed in this study calls for not only the initial rock composition, but also that of the residual and the melt to be known. This limited the use of the model to rock compositions that had been examined with experiments. Recognizing this shortcoming, attempts were made to duplicate the output of experimental partial melts to assess the aptitude of the MELTS program for melting crustal composition rocks (see Section 3.1).

CHAPTER 3

INFLUENCE OF SOURCE COMPOSITION ON MELT CHEMISTRY

Several parameters can affect melt chemistry. This chapter explores the most important of these factors. First, I discuss the influence of source rock composition and the critical need for partial melt compositional data for predicting isotopic disequilibrium. Following this, I present modeling results that provide insight into the influence of protolith age. Finally, I discuss the role of accessory phases and water on melt generation and composition.

3.1. MELTS Modeling

To compensate for the lack of partial melt data available, the MELTS algorithm was used to generate theoretical melts and residuals from source rock compositions. MELTS can be run through an online applet or more stably with the pHMELTS algorithm in MELTS mode (Ghiorso & Sack 1995, Asimow & Ghiorso 1998, Smith & Asimow 2005). In addition to being more stable, pHMELTS can be run with the *adiabat_1ph* program using a Perl script allowing the user to control more aspects of the melting conditions. Input files are created for the initial rock composition and the environmental variables (or melting conditions); these files are then called up by the *adiabat_1ph* program where the mineral modes and melt composition stable under those conditions is calculated.

MELTS can be used to determine assemblages along a set thermodynamic path or at a specific place in pressure-temperature space to investigate continuous, fractional, or batch melting and crystallization of the magma. Compositions may be examined at subsolidus or subliquidus conditions up to 3 GPa. MELTS is calibrated for compositions in the SiO_2-TiO_2-Al_2O3-Fe_2O_3-Cr_2O_3-FeO-MnO-MgO-NiO-CoO-CaO-Na_2O-K_2O-P_2O_5-H_2O system. Water is treated as an oxide component because it can readily go into the melt, hydrous minerals, and water vapor. Melt compositions may be water-saturated, -undersaturated, or anhydrous with the option of buffering the oxygen fugacity (fO_2) and the water activity (aH_20) of the system. A previous study comparing MELTS to experimental studies on peridotite melting has shown that there is a temperature offset (Hirschmann *et al.* 1998). A systematic ~100°C offset was seen with mantle melting conditions and compositions; the greatest inaccuracies were associated with calculating SiO_2 and MgO contents, as well as the size of the melt fraction.

Three compositions from partial melt experiments were modeled with pHMELTS to determine the utility of the program for melting crustal rocks, with the hope that if it performed well then it could be used to model compositions where experimental data were lacking. Two of the compositions were the same as used above (sources MW and MS) and the third, SMAG, was from Patiño Douce and Beard (1996), which has an identical modal composition to MW but contains biotite that is more Mg-rich. All experiments were run at 10 kbar with fO_2 approximately at QFM-1 (quartz-fayalite-magnetite reduction-oxidation

buffer). The buffer constrains the fO_2 of a system to a particular oxidation state, which can determine minerals that may form and their compositions. The experiments were restricted to QFM-1 or one log unit below the fO_2 for QFM at that temperature. Accordingly, all pHMELTS runs were done at the pressure and fO_2 conditions used in the experiments. Fig. 10 and 11 show the model against the experimental results for partial melts from composition SMAG, which demonstrated the best agreement (results for MS and MW can be found in the Appendix, Fig. A4-A7).

As was observed by Hirschmann *et al.* (1998), offsets were seen between the amounts of melt generated in experiments compared to pHMELTS (Fig. 10). The temperature differences typically ranged from 50-75°C, but did not appear to fluctuate according to a trend nor were they uniform between rock compositions. However, for the same degree of melting pHMELTS reported consistently lower temperatures than those seen experimentally. The amount of melt produced at a given temperature was most accurately modeled with composition MW (Appendix, Fig. A5). The melt and residual compositions for this rock, however, do not agree (Appendix, Fig. A7); no biotite or plagioclase was reported in the residual at any stage during melting, despite the fact that they comprise almost 65% of the original rock (Appendix, Table A3).

The oxide compositions of the melts generated by pHMELTS were compared with those from the experiments to determine the accuracy of the program (Fig. 11). The melt compositions were also examined for systematic trends that could potentially be calculated. No discernable patterns were observed in oxide

concentrations; the pHMELTS program determines higher concentrations for some and lower for others. Similar to the temperature offset seen, the variation is erratic and differs between rock compositions. For example, Al_2O_3 concentrations calculated by pHMELTS for SMAG (Fig. 11) and MW (Appendix, Fig. A7) were lower than those seen experimentally, but higher for MS (Appendix, Fig. A6). The only oxide that was consistently within ~10% of the experimental value was SiO_2. Hirschmann *et al.* (1998) also observed discrepancies between experiments and MELTS in partial melt compositions from peridotites. MELTS produced melt compositions with higher MgO and TiO_2 contents but lower SiO_2 than were observed experimentally; additionally, NaO concentrations for near-solidus partial melts were routinely overestimated.

Overall, pHMELTS was not able to reproduce partial melt data for any of the compositions examined. Consequently, it was determined that for crustal rocks pHMELTS is not a viable model and was not used to model any additional source rocks. Investigation of the compositions of residual phases calculated suggests that a major source of discrepancy between model and experimental results is that water is not partitioned into muscovite. After just small degrees of melting (<10%) muscovite and biotite are often prematurely removed from the residual; instead large amounts of potassium feldspar and aluminosilicates are reported in its place, suggesting that potassium and aluminum are reapportioned to different phases. Additionally, water does not appear to be appropriately distributed to micas.

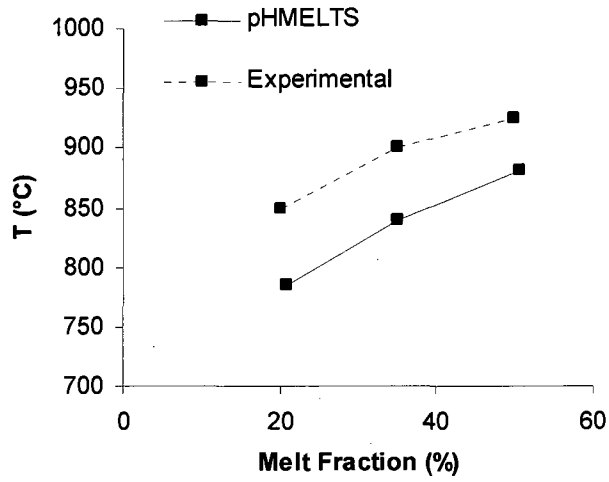

Fig. 10. Amount of melt produced from composition SMAG versus temperature. Experimentally determined by Patiño Douce and Beard (1996) and theoretically with pHMELTS.

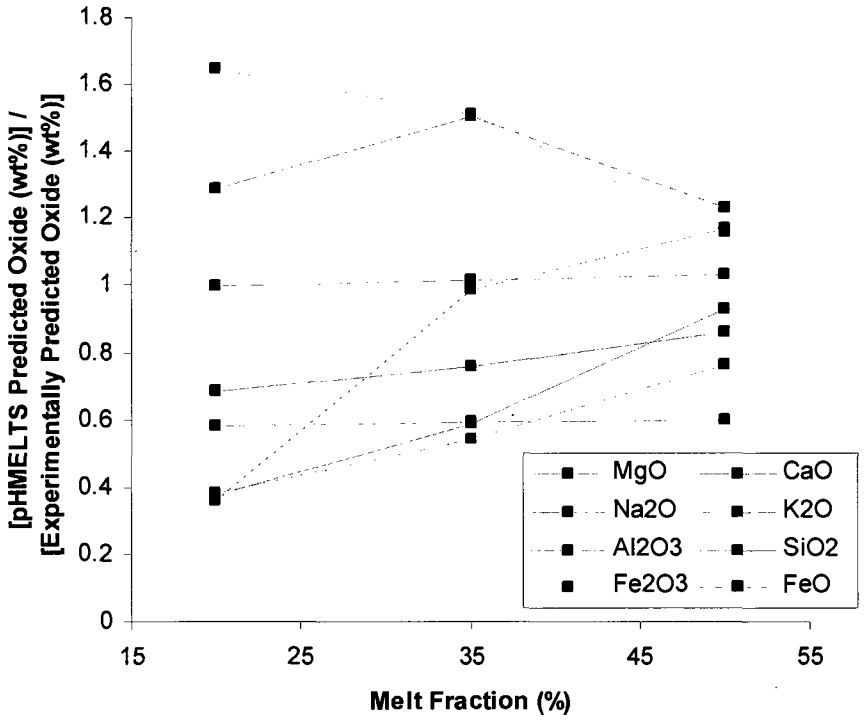

Fig. 11. Oxide composition of melts from SMAG as a ratio of the value predicted by pHMELTS and experiments (Patiño Douce & Beard 1996). Experimental FeO and Fe_2O_3 contents were calculated from FeO_{TOTAL} using MELTS (Ghiorso & Sack 1995). TiO_2 ratios ranged from ~1.5-3.2 and MnO ranged from ~8-17.

3.2. Effect of Protolith Age

When a rock first crystallizes the minerals it contains will have the same U-Th-Pb, Sm-Nd, and Rb-Sr isotopic ratios (in those minerals containing these elements). As each mineral becomes a closed system their isotopic ratios will begin to evolve according to the radioactive decay of each isotopic system and the concentrations of each element involved. Assuming the systems remain closed, through the course of time, minerals are able to progress to very different isotopic ratios (as shown schematically in Fig. 12). The differences in isotopic ratios that develop between phases are why partial melting is of great consequence. If all minerals had the same ratios then it would not matter which were entering the melt, but since they become increasingly diverse it is extremely important to understand what the isotopic signatures are of what is contributing to the melt. Thus, older rocks could potentially generate melts in even greater disequilibrium with their source rocks than younger ones of the same mineralogy (Hogan & Sinha 1991). Because melts produced from extremely old rocks may be considerably farther from equilibrium, they may also be able to remain in a state of disequilibrium for a longer period of time. Source composition MP with 0.01 wt. % zircon was modeled at 2.5, 1.7, and 0.5 Ga to illustrate how increasing the age of the protolith can amplify the amount of disequilibrium created (Fig. 13). As the age of the sample is increased the amount of disequilibrium calculated increases. Melts do not reach equilibrium for Nd and Pb due to apatite and zircon remaining in the residual until significant amounts of melting has occurred (see Section 2.2.2. for discussion and Fig. 5).

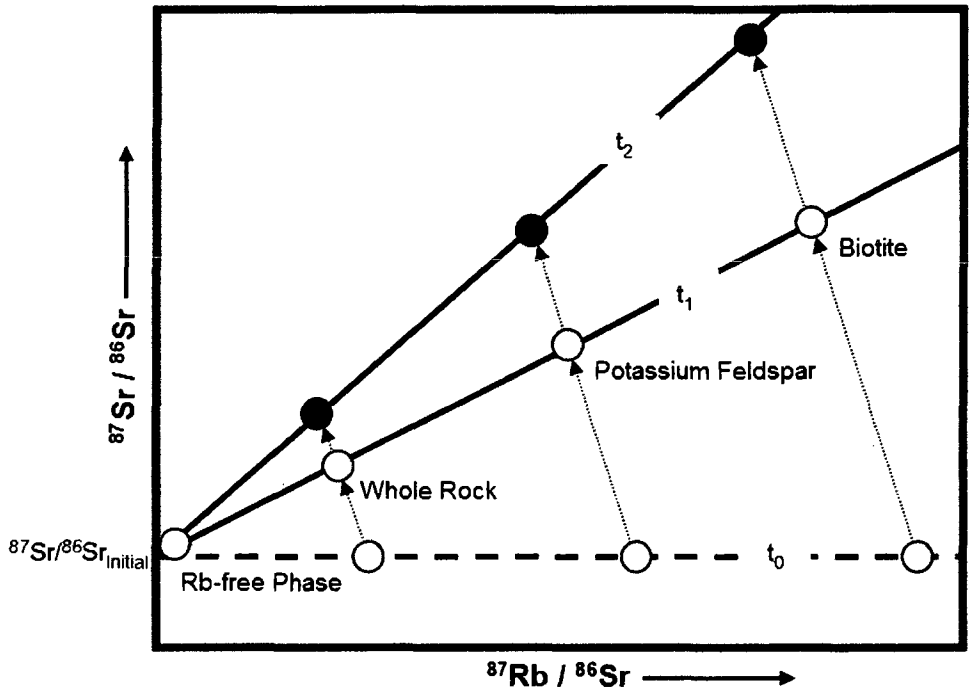

Fig. 12. Schematic of the Sr isotopic progression of several minerals contained in a theoretical whole rock composition (based on Fig. 3.4. in Dickin 2005). Initially (time t_0) every mineral contained in the rock has the same $^{87}Sr/^{86}Sr$ value but once each becomes a closed system the ratios evolve independently respective of the amount of ^{87}Rb decaying to ^{87}Sr. Over time, from t_0 to t_1 and t_2, the isotopic ratio if each mineral can become increasingly distinct.

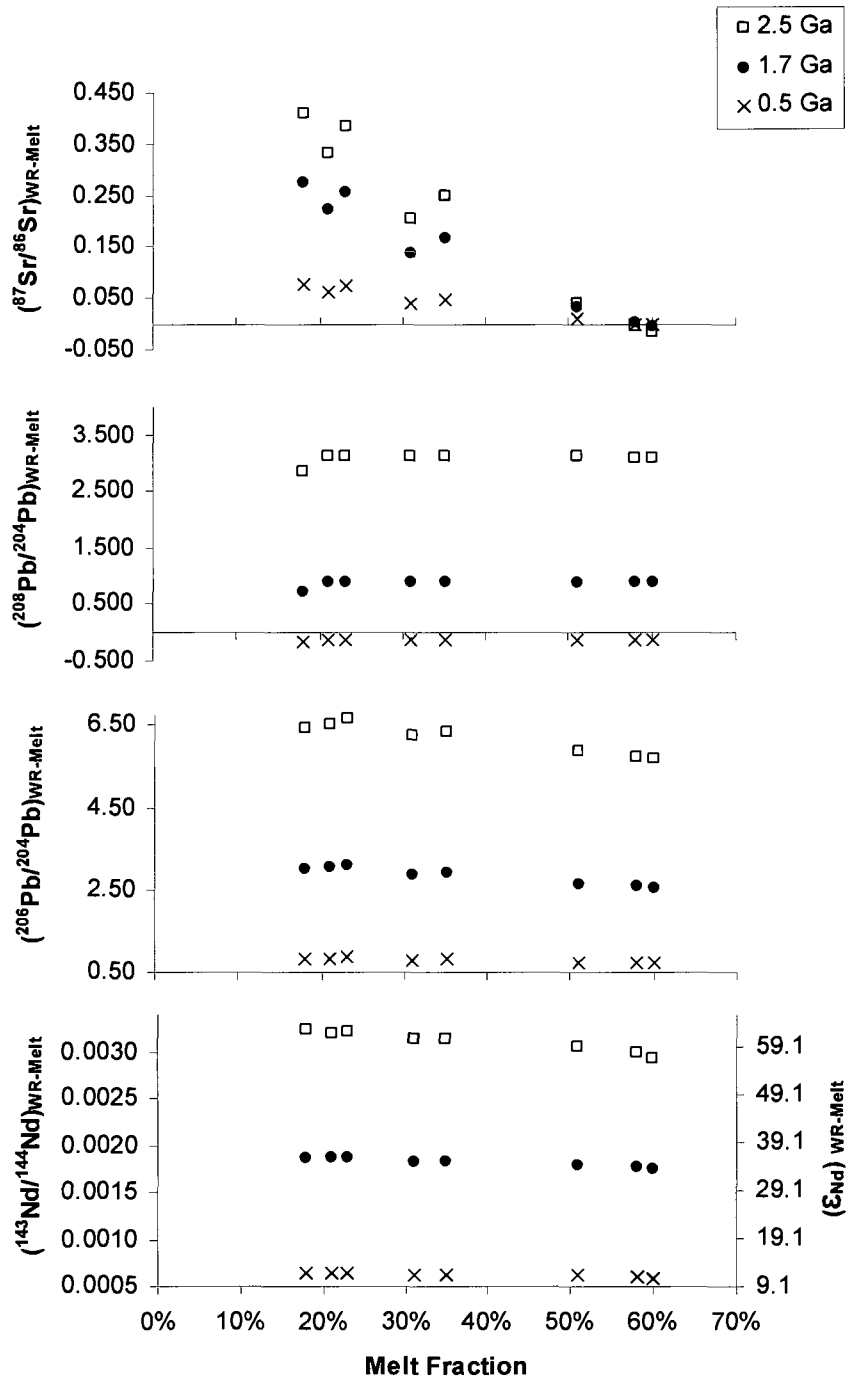

Fig. 13. Isotopic disequilibrium associated with MP composition rocks (0.01 wt. % zircon) with ages of 2.5, 1.7, and 0.5 Ga. Disequilibrium is expressed as the difference between the isotopic ratio of the whole rock (WR) and the partial melt.

3.3. Role of Accessory Phases

As briefly discussed in earlier sections and demonstrated by the model created in this study, accessory minerals have an intimate relationship with the elements used as tracers of magmatic processes. Because many incompatible elements strongly partition into these phases, residues are able to retain these elements when the minerals holding them are relatively insoluble. The concentrations of Zr and some REE's in the melt have been utilized as indicators of the extent to which certain minerals are dissolving into the melt (e.g. Watson & Harrison 1983, Montel 1993). The effectiveness of a phase to hold on to its trace element supply is controlled by four main parameters: the solubility of the mineral into melts; the diffusivity of the element in the mineral, which determines the rate at which equilibrium between phases and melt still in contact may be reached; the partitioning of elements and isotopes between minerals and the melt (Watson & Harrison 1984); and the kinetic effects of melting. Additionally, the positions of the accessory mineral grains within the rock are important in assessing their ability to contribute to melts. If the phases are shielded from involvement in melting, such as those held as inclusions in large grains of minerals not involved in the melting reaction, the resultant melts may have unusually low Zr and REE concentrations (Watt & Harley 1993). However, crustal melts often contain P and Zr reflecting zircon and apatite saturation indicating that they are able to communicate with the melt and are not isolated in the parent rock (White *et al.* 1977, Watson & Harrison 1984). Observations of individual grains, such as sub-rounded cores on zircons, further suggests that accessory phases are often in

contact with the melt (Poldervaart & Eckelmann 1955, Watson & Harrison 1984). Those grains included in phases entering the melt and those located along grain boundaries are, of course, free to go into the melt according to their solubility (Watson & Harrison 1984, Watson *et al.* 1989). Despite evidence that accessory phases are able to interact with the melt, trace element and isotopic equilibrium between melts and undissolved grains of accessory minerals is rarely reached (Watson & Harrison 1984, Watt & Harley 1993). While the dissolution of zircon, apatite, and monazite have been more extensively studied (Watson 1979, Watson & Capobianco 1981, Green & Watson 1982, Harrison & Watson 1983, Watson & Harrison 1983, Rapp & Watson 1986, Pichavant *et al.* 1992, Ayers & Watson 1993, Montel 1993, and others), the effects of other accessory phases of recognized importance to trace element budgets (namely titanite, allanite, epidote) are not as well constrained.

3.3.1. Apatite and Monazite

Experimental studies have convincingly demonstrated that apatite is generally an insoluble phase in crustal felsic melts (Watson & Capobianco 1981, Harrison & Watson 1984, Pichavant *et al.* 1992, and others). Source rocks with P_2O_5 levels above that required to saturate the melt will result in residual apatite; felsic melts from 750-900°C require up to 0.14 wt% dissolved P_2O_5 for saturation (Fig. 14(A)). Compositions containing less than 0.14 wt% P_2O_5 allow apatite to be consumed during melting. Those with as little as 0.05 wt% P_2O_5 have residual apatite until 35% melting; when source P_2O_5 is doubled apatite remains in the

residue until ~70% melting (Fig. 14(B)). The effects of apatite on REE budgets of crustally derived melts is most prominent for compositions containing more than 0.14 wt% P_2O_5 where garnet and/or amphibole are either in low abundance or not present in the residual (Watson & Capobianco 1981).

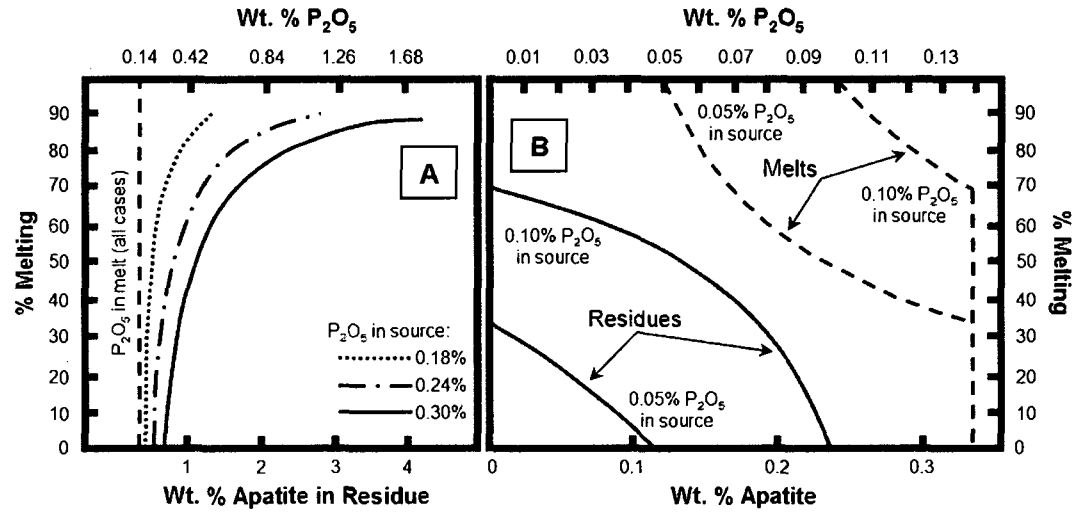

Fig. 14. Apatite and P_2O_5 contents of melts and residuals versus the percent of melting for sources with (A) 0.18, 0.24, 0.30 wt% P_2O_5 and (B) 0.05 and 0.10 wt% P_2O_5 (Fig. 1. from Watson & Capobianco 1981).

As discussed in previous sections, apatite and monazite may have competing dissolutions due to P being a structural component in each. During dehydration melting, monazite becomes relatively insoluble and stays in the residual even when apatite is not present to inhibit dissolution. Additionally, monazite becomes less soluble with increasing silica content (Montel 1986). In peraluminous rocks, monazite is likely to be the most common REE-bearing mineral due to low CaO concentrations hindering apatite, sphene, and allanite stability (Watt & Harley 1993). The fact that most continental crust contains LREE concentrations sufficient enough to saturate peraluminous melts also fosters the formation of

monazite (Miller & Mittlefehldt 1982, Watt & Harley 1993). Larger monazite grains (> 100 μm diameter) may take more than ~10 million years to dissolve in the melt concentrating it in the residual, while smaller grains (~10 μm diameter) may dissolve as quickly as 50,000 years (Rapp & Watson 1986).

3.3.2. Zircon

The major restraint on the formation of zircon and its ability to dissolve into melts is the Zr concentration of the source rock. Generally, 60 pmm of Zr is enough to saturate a melt and leave zircon in the residual (Watson 1988). Due to the fairly insoluble nature of Zr, the concentration required to saturate the melt is low (Weber & Barbey 1987). Beyond the influence of Zr, the behavior of zircon is particularly affected by temperature, silica content, and the presence of water (Watt & Harley 1993). At higher temperatures zircon becomes more soluble, however, in increasingly felsic melts it becomes more insoluble (Watson & Harrison 1984, Watson 1988). For hydrated melts (> 1.5-2.0 wt% H_2O) the solubility of zircon becomes independent of water content, however, for drier felsic melts there exists a relationship between zircon solubility and water content; crustal melts with only 0.02 wt% H_2O may dissolve 30-40% less zircon than ones containing 2.0 wt% H_2O (Watson & Harrison 1983). Consequently, during dehydration melting, the focus of this study, zircon is able to stay mostly in the residual, as illustrated in Fig. 15. Melt compositions from Knesel and Davidson (1999) and the zircon solubility equation (Watson & Harrison 1983) were used to calculate the amount of zircon that would be able to enter the melt

for sources with 0.01, 0.03, 0.05, and 0.10 wt. % zircon (see Table A8 in Appendix for values used and calculated). Since partial melt data were available for 56-77% melting, it was assumed that at 99% melting the major cation chemistry of the melt produced would be approximately the same composition as the whole rock. This allowed for a more complete view of how zircon would partition into a felsic melt.

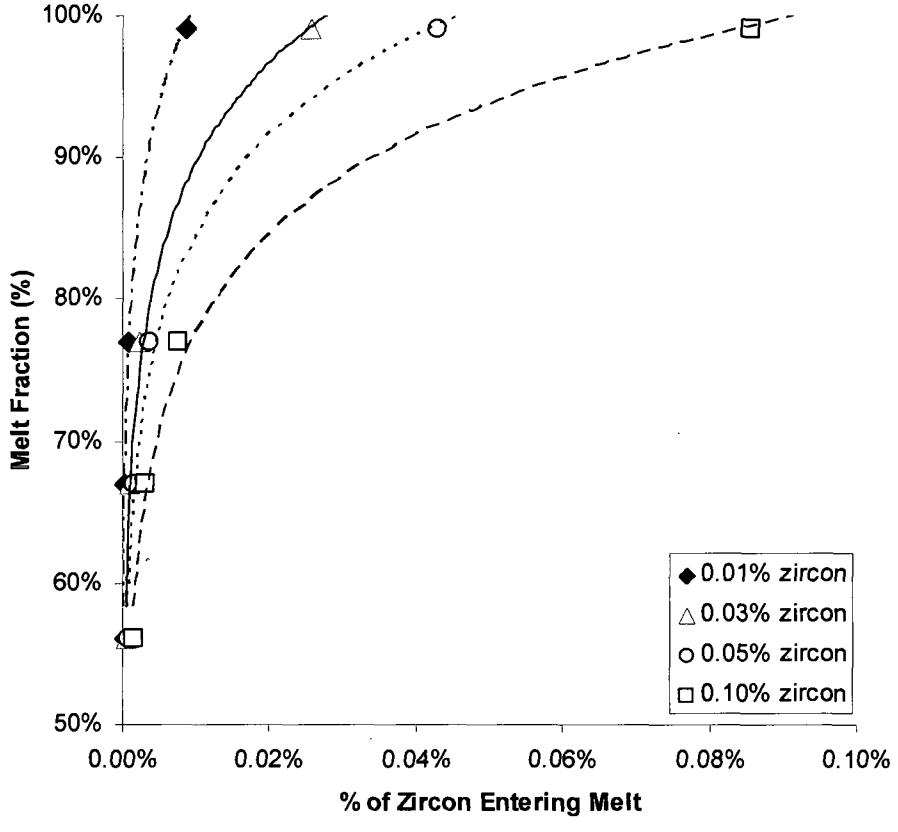

Fig. 15. The amount of zircon calculated to enter into a felsic melt from a biotite granite with varied percentages of zircon (Watson & Harrison 1983, Knesel & Davidson 1999).

3.4. Influence of Water

The effect that the presence of water in source compositions has on individual accessory phase minerals has been discussed, but it can also have significant implications on the mineral break down reactions driving melting in crustal rocks. Water not only lowers the solidus of quartz + plagioclase but it also stabilizes muscovite (Zeng *et al.* 2005(a)). During dehydration melting micas serve as the source of water causing the melting reaction and consequently muscovite breaks down in greater amounts compared to plagioclase. The addition of water to a system restricts the capacity of muscovite to contribute to melt formation, allowing plagioclase to break down in larger proportions than muscovite (Patiño Douce & Harris 1998). For example, Patiño Douce and Harris (1998) demonstrated that under the same pressure and temperature conditions (6kbar and 750°C) the addition of 2 wt% changed the melting reaction from that described by Eq. 9 to:

Wet Melting: $Ms + Pl + Qtz + H_2O \rightarrow Melt$ **(10)**

They also noted that the ratio of muscovite to plagioclase changed from 22:7 during dehydration melting to 9:15 during water-fluxed melting (mass proportion ratios). The proportion of these two minerals to each other during wet melting is also influenced by the pressure and temperature conditions; higher pressures and lower temperatures favor plagioclase dissolution while higher temperatures enhance the consumption of muscovite (Patiño Douce & Harris 1998).

CHAPTER 4

PRELIMINARY EXPERIMENTS

To complement the theoretical component of this study, partial melt experiments were conducted. These introductory experiments allow the relationship between rock textures and melt generation to be assessed. Observations of introductory experiments on a sample representing a typical crustal rock, which contains accessory phases of interest, suggests that the partial melts formed could potentially be in considerable disequilibrium with the whole rock.

4.1. Sample Information

A sample, collected and donated by Dr. Samuel A. Bowring (M.I.T.), from the Hualapai Mountains in Arizona was used as starting material for piston-cylinder experiments (Fig. 19). This region is part of the Yavapai Province which is broken up into tectonostratigraphic blocks: the Hualapai-Bagdad, Green Gulch, Big Bug, and Ash Creek blocks. These blocks are believed to have been emplaced ~1.7-1.8 Ga by thrusting and strike-slip movement along shear zones between the blocks. The Mojave Province, located to the northwest, is thought to have been juxtaposed into position around the same time while the Mazatzal

Province, to the southeast, is believed to have been emplaced from 1695-1630 Ma (Karlstrom & Bowring 1988).

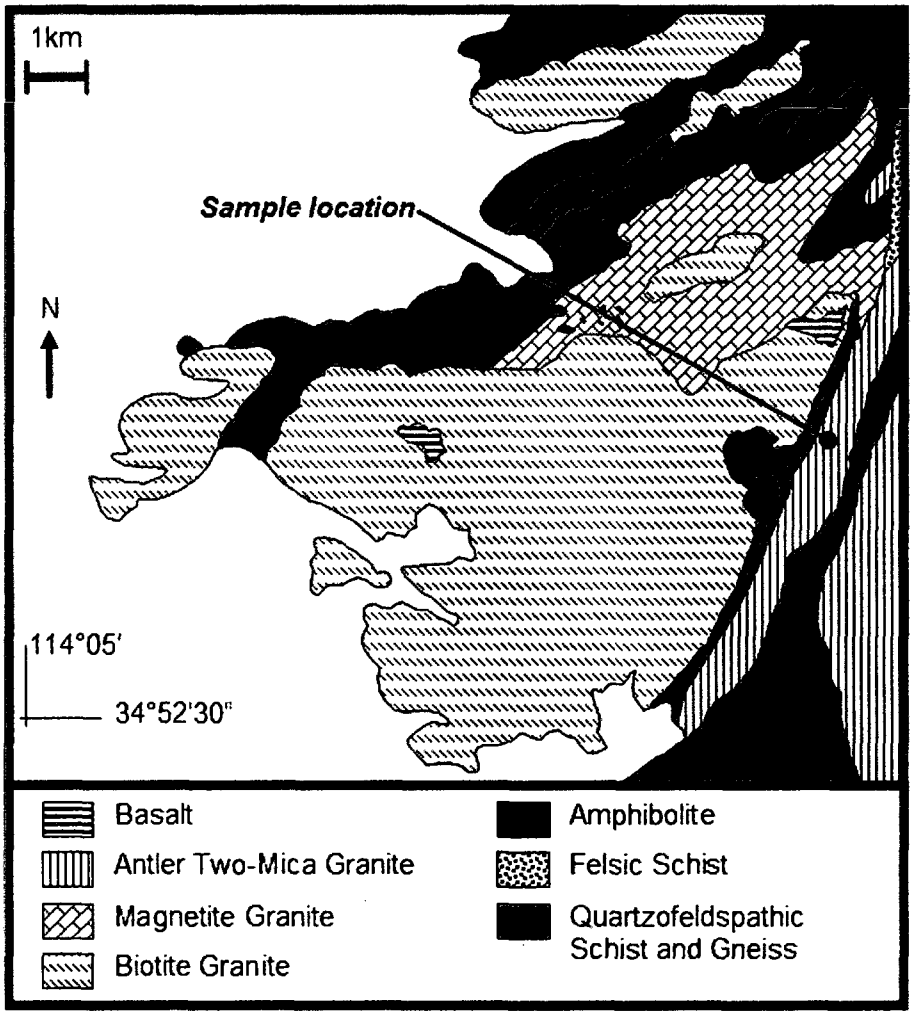

Fig. 16. Generalized geologic map of sample location in the west-central Hualapai Mountains, AZ (adapted from Chamberlain & Bowring 1990 and Conway *et al.* 1989).

Rock types in the west-central area of the Hualapai Mountains where the sample was taken include schists, gneisses, amphibolites, and granites. Most of the metamorphic rocks cropped out in this area are abundant in quartz and micas and are fine-grained; these rocks are frequently cut by granitic plutons,

pegmatites, and basaltic intrusions (Strensrud & More 1980, Conway *et al.* 1990). The rock unit sampled was the Antler two-mica granite located in the Boriana Canyon of the Hualapai Mountains (Fig. 16). Zircon geochronology of the sample yielded an age of 1694 ± 14 Ma (Chamberlain & Bowring 1990), while apatite recorded slightly younger U-Pb ages of 1609-1731 Ma and Pb-Pb ages of 1515-1568 Ma (Chamberlain & Bowring 2000).

4.2. Mineralogical and Petrographic Description

The Antler granite (of Fig. 16) is referred to as a two-mica granite indicating the presence of both muscovite and biotite. This unit is more muscovite-rich to the northeast and biotite-rich to the southwest (Strensrud & More 1980); on the whole, biotite is the dominant mica over muscovite and potassium feldspar is the dominant feldspar over plagioclase. The sample used in this work (AZ244, also used in Chamberlain & Bowring 1990, 2000) is a medium- to coarse-grained granite with phenocrysts of potassium feldspar up to 10 mm across. It is composed of approximately 40% potassium feldspar, 30% quartz, 15% biotite, 10% plagioclase, 5% muscovite, and accessory phase (<1%) apatite, zircon, and oxides.

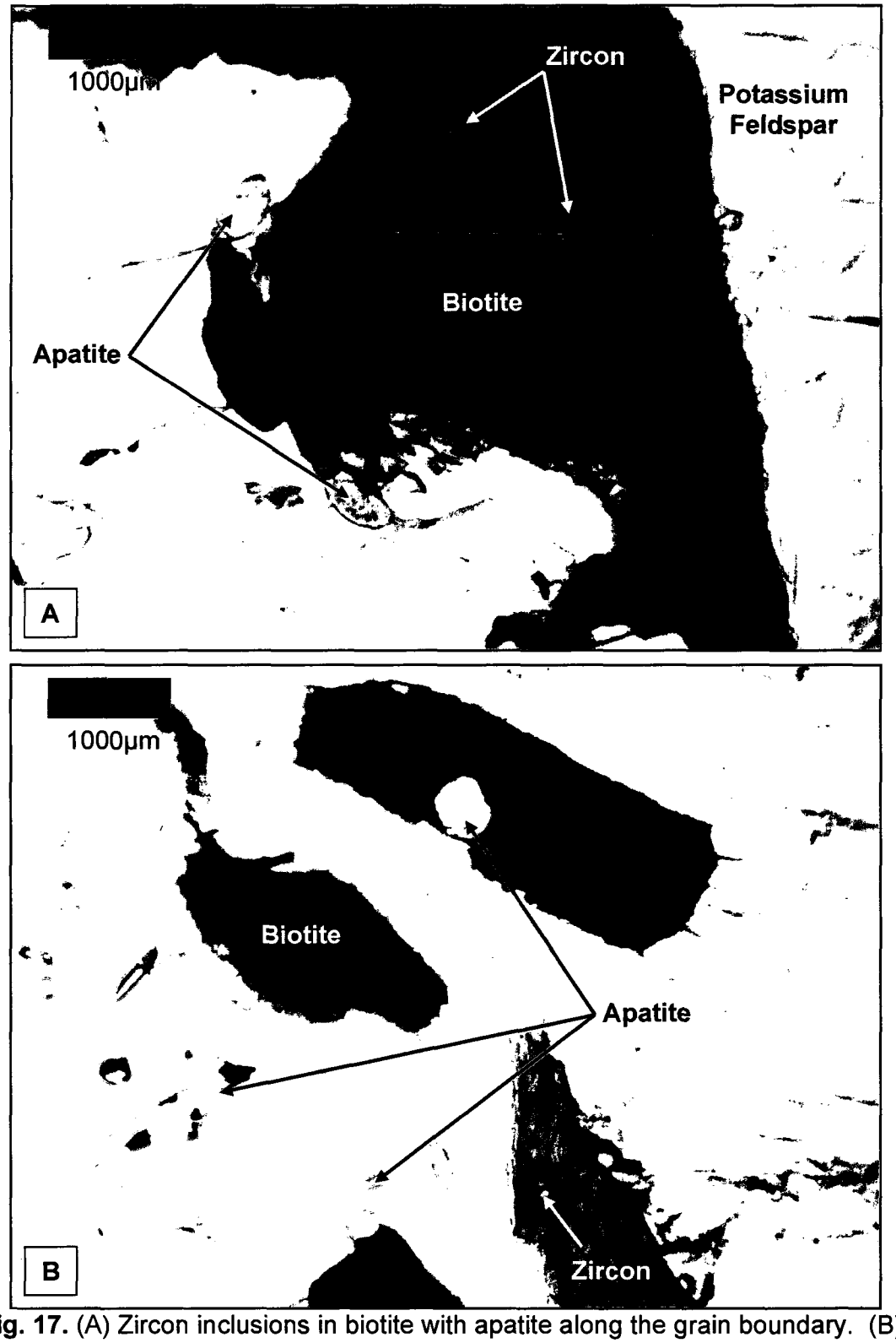

Fig. 17. (A) Zircon inclusions in biotite with apatite along the grain boundary. (B) Apatite included in biotite and between grains of potassium feldspar and quartz.

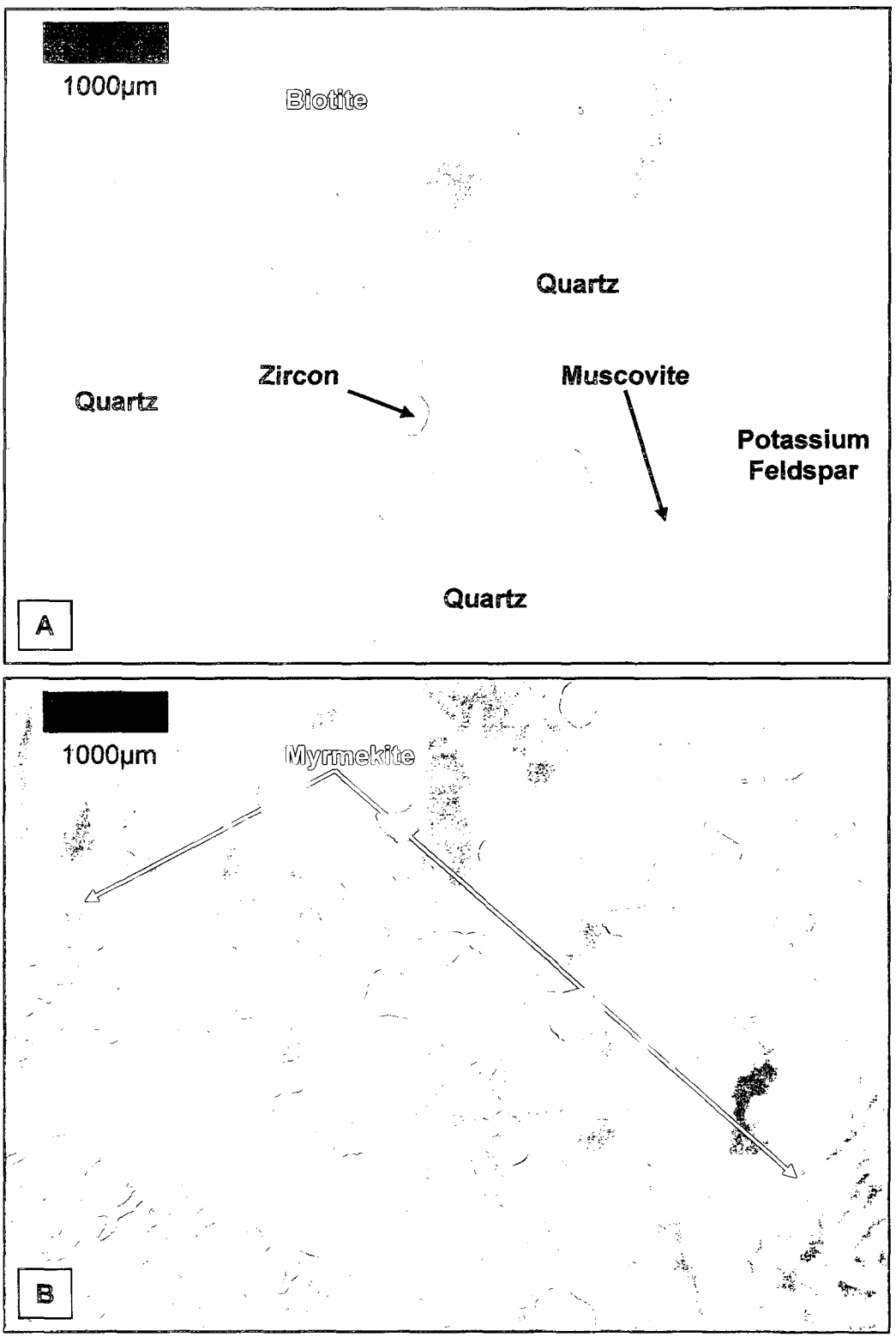

Fig. 18. (A) Zircon grain along the grain boundary between biotite and quartz. (B) Myrmekite formed in feldspar grains.

In this sample, apatite is an abundant accessory mineral and is normally located along grain boundaries (Fig. 17(A)), but can be included in other phases such as biotite (Fig. 17(B)). Zircon is typically found as inclusions in biotite (Fig. 17), although it is also seen along grain boundaries (Fig. 18(A)). Myrmekite, a vermicular intergrowth of quartz in sodic plagioclase, was also observed in minor amounts throughout the sample (Fig. 18(B), Nold 1984). Major and trace element concentrations were determined via X-ray fluorescence (XRF) and inductively-coupled-plasma mass spectrometry (ICP-MS) by the Washington State University GeoAnalytical Lab (see Appendix, Tables A9 & A10 for results).

4.3. Experiment Setup and Design

To simulate partial melting at crustal pressures and temperatures, solid-media piston-cylinder apparatuses at Rensselaer Polytechnic Institute (RPI) were utilized. With the aid of Dr. Bruce Watson, experiments were designed to generate and capture melts from natural whole rock starting materials. As depicted in Fig. 19, ~30 mg of 45-53 μm diamonds were loaded on top of ~50-60 mg of 106-149 μm crushed rock sample in a sample capsule made of graphite and silver. The diamonds were cleaned in trace element grade nitric and hydrochloric acid, followed by optima grade nitric acid to leach out any potential impurities. Ideally, all melt produced will migrate up and into the pore space between the diamonds, allowing for it to be more easily analyzed. Similar sample capsule designs have been used by Knesel and Davidson (2002) and Baker and Stolper (1994).

The capsule is put inside of a series of compressible layers before being placed into the piston-cylinder apparatus (Fig. 19). There are several magnesium oxide cylinders enclosing the sample capsule: a solid one placed beneath it, another hollowed out which surrounds it, and a third located above the capsule which has a small hole drilled out of it. The tube in the uppermost magnesium oxide cylinder is designed for holding a thermocouple, which monitors the amount of current running into the sample cell and therefore the temperature of the experiment. A thermocouple is composed of rhenium-tungsten wires laced inside of thin corundum tubing. Because a thermal gradient exists in each sample cell, the height of each piece of magnesium oxide layer is designed so that the sample is located at the vertical center where there is the least variability in temperature. Below the magnesium oxide is a cylinder of Pyrex glass and a graphite disk, and surrounding it is a tube of graphite and Pyrex glass, salt, and lead foil. The graphite works to conduct electricity through the experiment while the salt insulates the sample cell from the rest of the metal apparatus, ensuring that current is only running through this area. Additionally, sheets of vellum are used to insulate the layer of the piston-cylinder where the sample capsule is held; the lead foil allows the cell to be easily slipped into a cylindrical cavity in this layer.

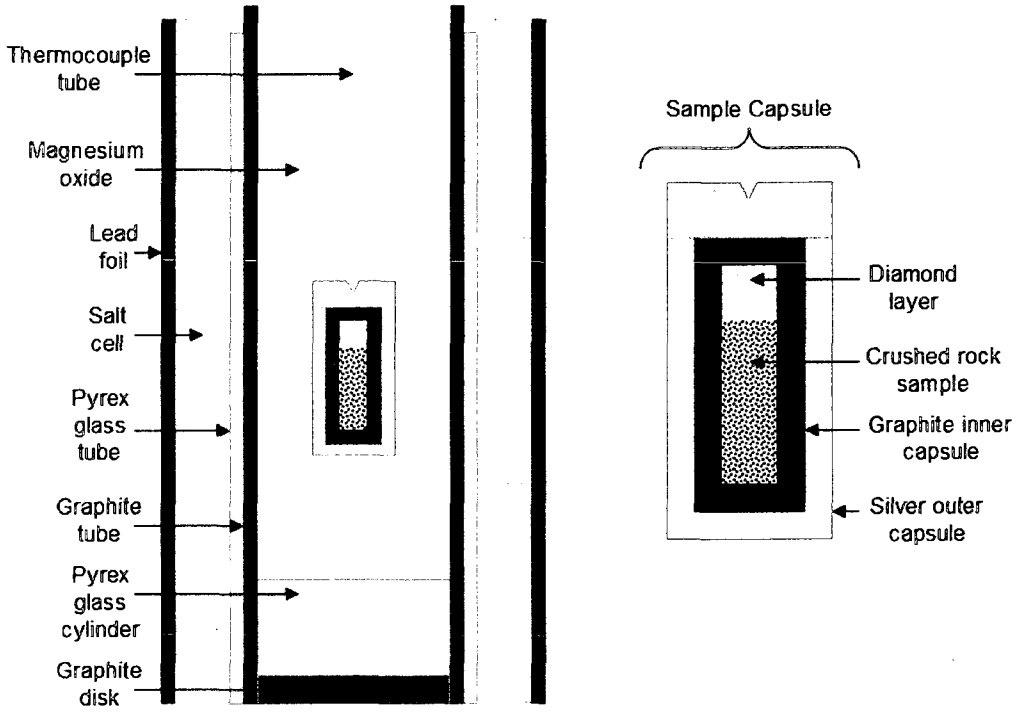

Fig. 19. Schematic of sample cell and capsule design used in piston-cylinder experiments conducted.

Several preliminary experiments were conducted at 10 kbar, varying temperatures, over ~24 hours to establish the effectiveness of melt generation and capsule design in capturing melts. At 750°C no discernable melt was observed, although some grains appeared to be slightly rounded (Fig. 20(A)). This experiment was also run using a capsule design which had three sample wells and no graphite lining between the rock and the silver; based upon the results of this trial the aforementioned capsule was created. The graphite was added after the difficulties of extracting the sample with a minimal contamination was realized. It was also determined that a thicker layer of diamonds was needed for runs producing significant amounts of melt.

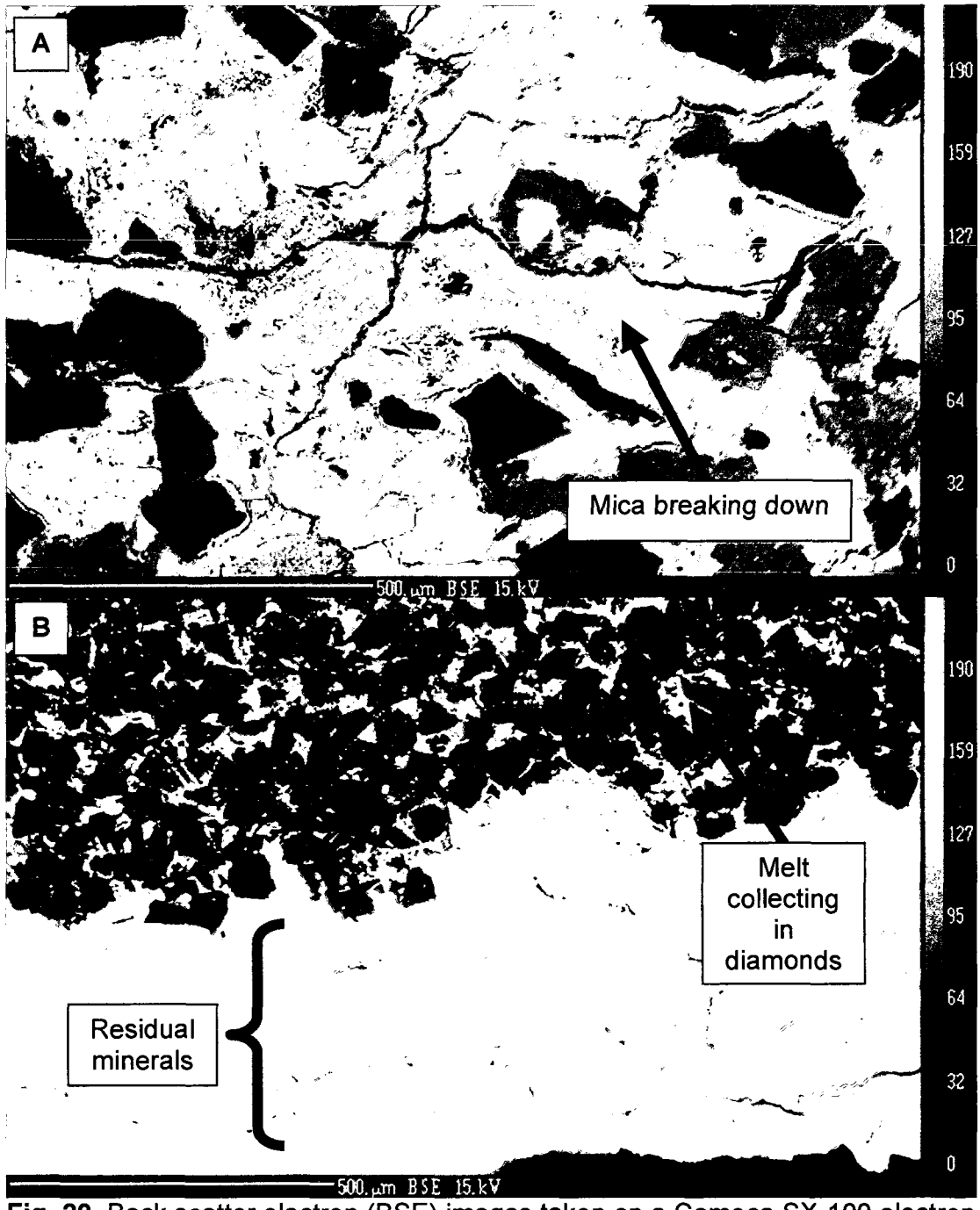

Fig. 20. Back scatter electron (BSE) images taken on a Cameca SX-100 electron microprobe of run products from experiments at 10 kbar and (A) 750°C and (B) 825°C. The white area prominently shown in (A) is biotite. The black grains at the top of (B) are the diamonds and the light grey material in between them is the melt generated. The grains of varying shades of grey are quartz, potassium feldspar, and plagioclase.

The ability of the melt to migrate into the diamond pore space was seen in the next trial ran at 825°C and 10 kbar (Fig. 20(B)). It was approximated by visual inspection that 5-10% melt was generated in this run and consequently the next one was done at 900°C and 10 kbar in order to produce slightly larger degrees of melting that could be more easily analyzed. Three experiments were carried out at 900°C, two for ~24 hours and one for ~6 days.

4.5 Melt Generation and Rock Texture

The presence of melt pooled in the pore space between the diamonds suggests that melt traveled along grain boundaries. The occurrence of accessory phases included within minerals involved in the melting reaction, namely biotite, and as individual grains implies that they would have had access to the melt forming. Accordingly, these minerals could have contributed to the composition of the melt. Additionally, the concentration of Zr (158 ppm) in the Antler granite is more than twice that necessary to saturate most melts (60 ppm, Watson 1988) and leave residual zircon. The concentration of phosphorus in the rock is 0.14%, which is the upper limit Watson and Capobianco (1981) found to be required for saturation of felsic melts (Fig. 14); for sources with 0.10% P_2O_5 apatite was able to remain in the residue until 70% had melted, implying that residual apatite would be present in the Antler granite during even larger degrees of melting. Taking all of these factors into account there is a high likelihood that apatite and zircon will be able to exert considerable influence on partial melts and cause them to be in isotopic disequilibrium.

CHAPTER 5

IMPLICATIONS OF ISOTOPIC DISEQUILIBRIUM

In this chapter, I present two quantitative models of crustal processes that illustrate the applications of the model I develop in Chapter 2. First, I model the assimilation of a partial melt into a basaltic magma body and discuss the additional insights that may be gained by this approach. Secondly, I explore a second potential application of my model, in considering partial melts which have undergone varying amounts of diffusive re-equilibration with their host rocks.

5.1. Assimilation of Partial Melts into Basalts

Due to the large amount of disequilibrium that can be created with just small degrees of melting, not accounting for it can have considerable repercussions on geologic interpretations. As discussed in Chapter 1, partial melts can be incorporated into magmas traveling through the crust. Accounting for this crustal contribution is important to understanding the cycling and transfer of material from the mantle to the surface of the Earth. Since Sr, Nd, and Pb are used to determine the mass input from the crust, assuming isotopic equilibrium between partial melts and their sources can lead to gross inaccuracies in volumetric estimations of crustal contaminant.

5.1.1. Limitations of Traditional Assimilation Models

Advances in analytical technology have enabled the examination of increasingly smaller scales (down to several microns). High spatial resolution measurements of trace element and isotope concentrations have allowed geochemists to further decipher the intricate processes occurring within the Earth's crust during magma transport to the surface. Coupled with models which assimilate crustal material into magma bodies, these data have enabled micro-scale determinations of the geochemical impact on magma compositions incurred by this process. The most commonly used models for this purpose are the assimilation and fractional crystallization (AFC, DePaolo 1981) and energy-constrained assimilation and fractional crystallization (EC-AFC, Spera & Bohrson 2001) models.

The AFC model attempts to simulate the trace element and isotopic effects of contemporaneous wallrock assimilation and fractional crystallization in a magma chamber. Both elemental mass and species are conserved while the melt fraction is an independent variable. Recharge of the magma chamber can also be accounted for with this model. Despite shortcomings this model may have, it is useful for describing the geochemical progression of magmas. The EC-AFC model enhances the AFC model by incorporating the concept of conservation of energy (sensible and latent heat effects) through thermodynamic parameters.

While both models have improved the parameterization of crustal assimilation, they do not adequately represent the isotopic influence of partially melted crust incorporated into the magma. Both models treat the magma and assimilant

isotopic compositions as bulk isotopic end member compositions that are mechanically mixed and fully equilibrated. Experimental and theoretical work, however, suggest that partially melted crustal material does not typically reflect the bulk isotopic signature of its source rock and that isotopic disequilibrium may actually be more prevalent than equilibrium (Gardien *et al.* 1995, Knesel & Davidson 1996, Harris *et al.* 2000, Knesel & Davidson 2002, Tommasini & Davies 1997). Because the AFC and EC-AFC models do not properly account for the isotopic effects of partial melting, this study and others have attempted to create models correcting this (e.g. Hogan & Sinha 1991, Davies & Tommasini 2000, Zeng *et al.* 2005(a)).

5.1.2. Bulk Rock versus Partial Melt Contamination

The incorporation of crustal material into basaltic magmas can have significant effects on the isotopic composition. Assuming that the assimilant has the isotopic signature of the bulk rock can lead to inaccuracies when determining the amount of crustal contamination that has occurred. Consequently, studies which calculate rates of crustal growth (e.g. Jacobsen 1988) or relative contributions from the mantle versus the crust in granitic magma bodies (e.g. Nelson & DePaolo 1985) may be erroneous. To demonstrate the isotopic disparities that may be seen between assimilating a melt with the whole rock composition versus that of a disequilibrium partial melt, a 51% melt from rock sample MP (see Chapter 2) and the bulk isotopic composition were mixed with a basaltic composition. Values used in the isotopic mixing calculations can be

found in Table 2; isotopic ratios are weighted by elemental concentrations when determining the signature of the mixture. An example for Sr is shown below:

$$\frac{^{87}Sr}{^{86}Sr_{Mix}} = \frac{\frac{^{87}Sr}{^{86}Sr_A}[Sr]_A f + \frac{^{87}Sr}{^{86}Sr_B}[Sr]_B(1-f)}{[Sr]_A f + [Sr]_B(1-f)} \quad \textbf{(10)}$$

where $^{87}Sr/^{86}Sr_{Mix}$ is the ratio of the mixture forming, $^{87}Sr/^{86}Sr_A$ is the ratio in component A, $^{87}Sr/^{86}Sr_B$ is the ratio in component B, and f is the fraction of A that is entering into the mixture.

Source	Pb	$^{206}Pb/^{204}Pb$	$^{208}Pb/^{204}Pb$	Sr	$^{87}Sr/^{86}Sr$	Nd	$^{143}Nd/^{144}Nd$	ε_{Nd}
Basaltic Magma	1.7	19.198	38.681	382	0.70396	30.1	0.512933	5.75
MP-Whole Rock (0% zircon)	1.97	18.919	37.260	41.2	1.03393	1.4	0.512867	4.47
MP-51% Melt (0% zircon)	1.35	16.615	36.569	30.6	0.75761	0.27	0.510916	-33.60

Table 2. Summary of elemental and isotopic data used for calculating isotopic mixing curves in Fig. 21 and 22. Values for the Basaltic Magma are from an Oligocene flood basalt from western Yemen (Baker *et al.* 1996). Nd values for the whole rock and partial melts were normalized according to DePaolo and Wasserburg (1976) and were converted to the Nd normalization scheme used by popular convention for calculations performed. MP isotopic values calculated using the model developed in Chapter 2.

The results of the isotopic mixing of melt with a basaltic magma are shown in Fig. 21 and 22. As indicated by the red arrows in these figures, the isotopic signatures of magmas contaminated by considerably larger amounts of melt with the whole rock composition correspond to smaller quantities of assimilated disequilibrium melt. For example, Fig. 21 shows that the ε_{Nd} value of a basalt is approximately the same, whether contaminated with ~30% whole rock composition or ~10% partial melt. Similarly, the assimilation of ~25% partial melt

may yield $^{208}Pb/^{204}Pb$ ratios analogous to basalts contaminated with ~40% bulk composition material; only ~10% disequilibrium melt is needed to produce $^{206}Pb/^{204}Pb$ ratios seen from the same ~40% whole rock composition melt. Because the ratio of each component mixing with the basalt is weighted by the relevant elemental concentration, the control each constituent is able to exert is heavily influenced by this. The assimilant composition used in this example had relatively low concentrations of the trace elements of interest, if a sample more enriched in Sr, Nd, and Pb had been used it could have potentially caused even greater changes in the isotopic signature of the basalt than those seen.

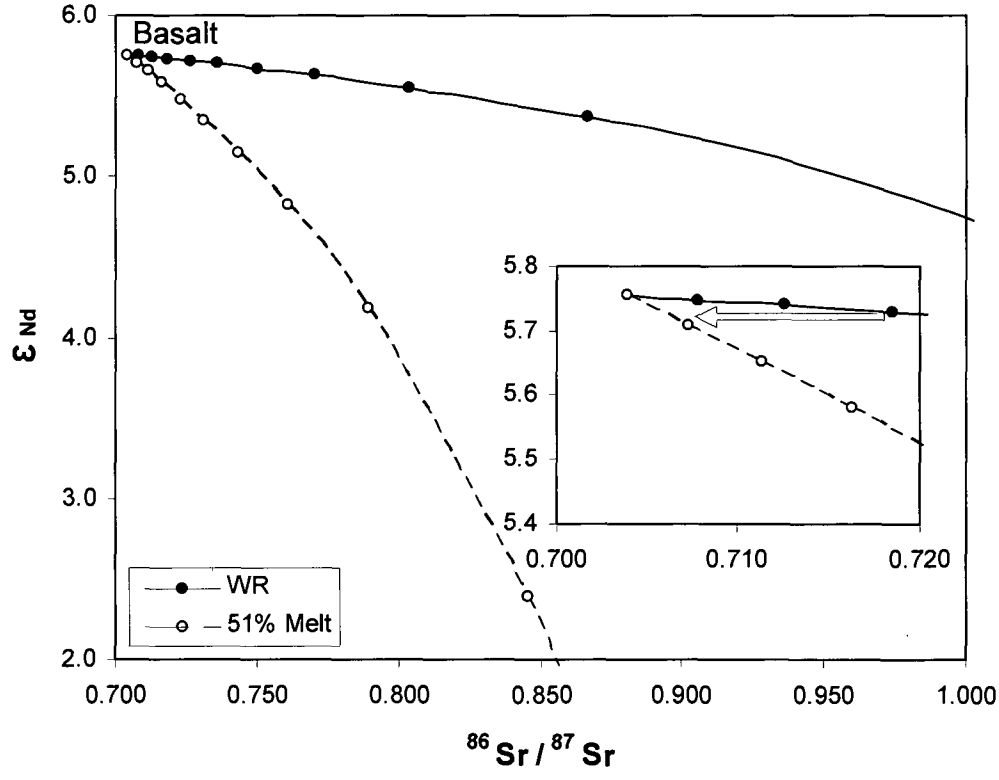

Fig. 21. Assimilation of material with whole rock (WR) isotopic composition and that of a 51% partial melt. Tick marks are at 10% intervals of material being incorporated into the basalt. Red arrow shows how larger percentages of whole rock contamination may potentially have identical isotopic signatures to basalts that incorporated smaller amounts of partial melt.

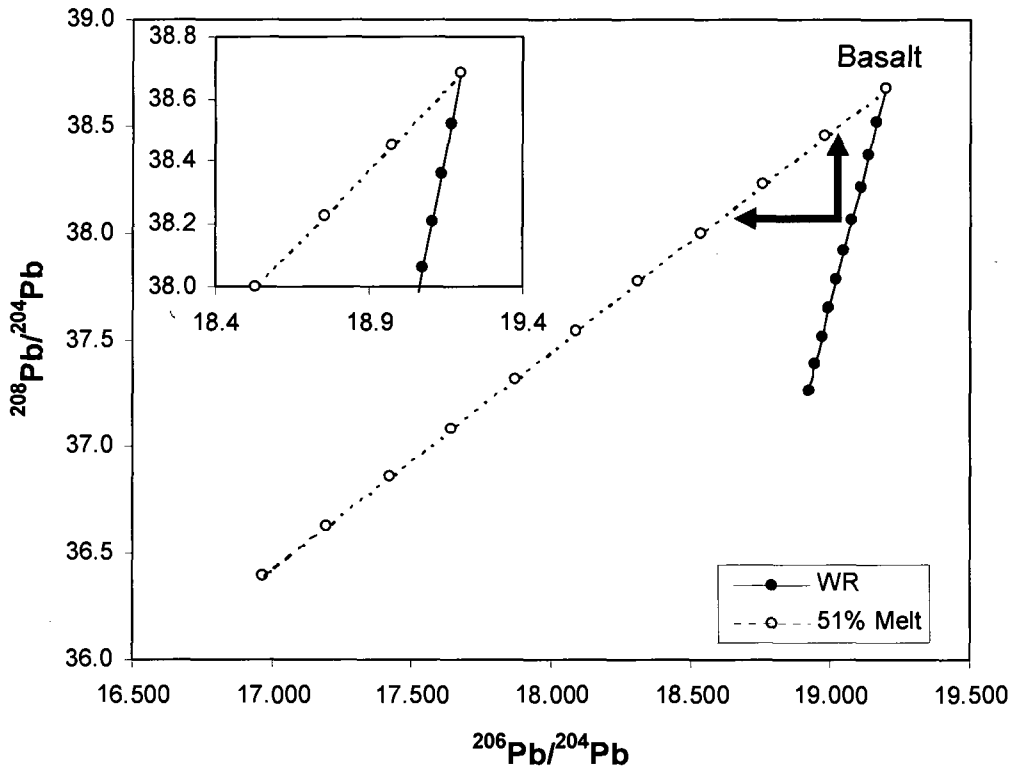

Fig. 22. Assimilation of material with whole rock (WR) isotopic composition and that of a 51% partial melt. Tick marks are at 10% intervals of material being incorporated into the basalt. Red arrow shows how larger percentages of whole rock contamination may potentially have identical isotopic signatures to basalts that incorporated smaller amounts of partial melt.

5.2. Diffusive Re-equilibration in Residual Phases

Partial melts in disequilibrium that remain in contact with their residual material following anatexis will progress back towards equilibrium with time. The period over which each isotopic system re-equilibrates is regulated by the rate of diffusion between the melt and the residue. Intra-crystalline diffusion in residual phases, however, likely controls the timescale over which melt-rock exchange can occur. Knowledge of the initial isotopic disequilibrium created allows for the amount of subsequent re-equilibration to be ascertained, which can in turn

amount of subsequent re-equilibration to be ascertained, which can in turn provide constraints on melt extraction rates. Offsets between isotopic systems in time required for re-equilibration can also contribute valuable information on melt residence time. This temporal parameterization has applications for understanding the nature of the lower crust and the process of migmatization where melts may reside in their source rocks for variable amounts of time prior to removal.

To illustrate the timescales over which these isotopic systems may re-equilibrate, experimentally-derived diffusion equations were combined with a crystal-liquid diffusive exchange model (used by Christensen & DePaolo 1993 and Bryce & DePaolo 2004, developed from Carslaw & Jaeger 1959). Because the diffusive re-equilibration of Sr can be controlled by several different minerals and also likely equilibrates before Nd, it was not modeled here. When plagioclase is present in large amounts it may control the re-equilibration of Sr; compositions lacking this phase, however, may be effected by other minerals such as biotite. The bulk composition of the material will influence how all three isotopic systems re-equilibrate but Pb and Nd in felsic crustal rocks are likely to be controlled by the behavior of the accessory phases (as shown with the case studies in Chapter 2). Accordingly, only the re-equilibration of Pb and Nd in apatite were modeled here and not Sr.

The phase most responsible for the disequilibrium created between the melt and the source rock is anticipated to regulate the progression of diffusive re-equilibration. While this accounts for the mineral expected to be the most

influential to each system, a more comprehensive and accurate approach should include the diffusion of these elements for all phases composing the rock. However, such a model is beyond the scope of this research and in this study a single mineral was focused on. In rock compositions examined in this study, residual apatite is primarily responsible for the disequilibrium observed in Nd and Pb. Corresponding diffusion equations were used to model the re-equilibration of Pb and Nd (Cherniak 2000 and Watson *et al.* 1985, respectively):

$$D_{Nd} = 2.4 \times 10^{-6} \exp(-348\ kJ/mol\ /RT)\ m^2/s \quad \textbf{(11)}$$

$$D_{Pb} = 0.035 \exp(-70{,}000\ cal/mol\ /RT)\ cm^2/s \quad \textbf{(12)}$$

where D is the diffusion of Nd and Pb in apatite and T is in Kelvin. Diffusive re-equilibration at 900°C was examined in this study. The diffusive exchange model used calculates the percentage of a theoretical spherical mineral grain that has re-equilibrated with a well-mixed melt surrounding it (Fig. 23, y-axis) based upon the isotopic ratio of the melt (R_{melt}), the crystal (R_{xtl}), and the average between them (R_{avg}). This is plotted against a non-dimensional parameter of Dt/a^2 (Fig. 23, x-axis), where D is the diffusivity in m^2/s, t is time in seconds, and a is the radius of the grain in meters. Values from this plot are then used with the trace element diffusion equations described above to determine the re-equilibration time of various size grains (Fig. 23, inset):

$$(t)_x = (Dt/a^2)_x \cdot (a_{grain}{}^2 / D_{element}) \quad \textbf{(13)}$$

where x denotes the percentage of the mineral that has equilibrated, $(t)_x$ is the re-equilibration time, $(Dt/a^2)_x$ is the x-axis value from the larger plot when "x" percent

of the grain has re-equilibrated, a_{grain} is radius of the mineral grain, and $D_{element}$ is diffusivity of the element of interest in the mineral being examined.

As demonstrated in the inset in Fig. 23, Pb in apatite is anticipated to re-equilibrate orders of magnitude times faster than Nd; for 40% of 1 mm grain of apatite to re-equilibrate Pb requires thousands of years while Nd may take on the order of ~10^5 years to re-equilibrate. Pb may be able to undergo considerable re-equilibration before Nd diffusion has even made an impact on the disequilibrium in its system. This provides convincing evidence that offsets between isotopic systems on their progression back to equilibrium are likely to be preserved in migmatic rocks. Furthermore, it suggests that during rapid melt extraction (~10^3 years, Sawyer 1991, Ayres *et al.* 1996) melts may easily be able to sustain isotopic disequilibrium for Nd, and possibly for Pb. Examining how the different isotopic systems reset is also relevant to understanding residence times of these melts during melting events.

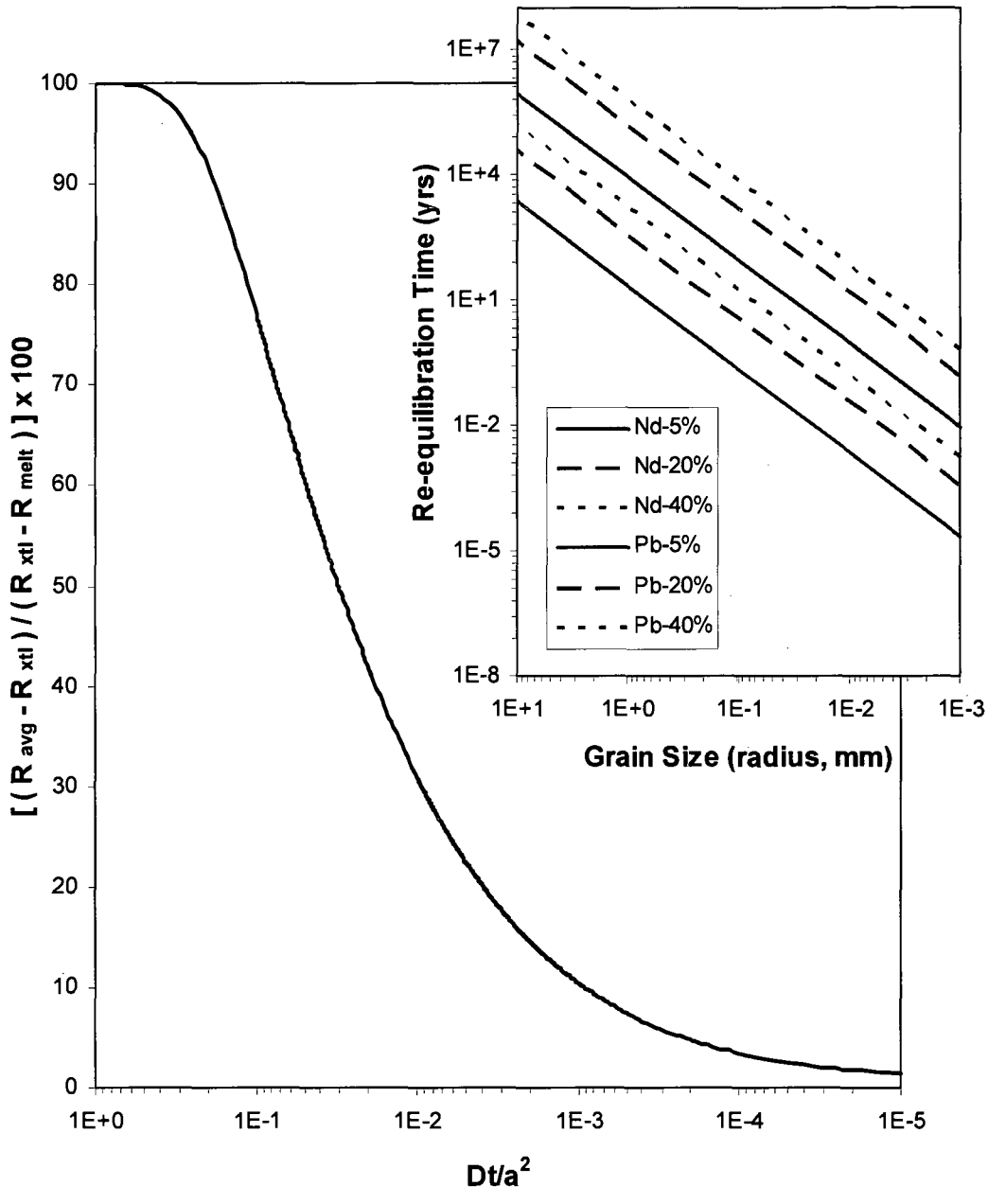

Fig. 23. Diffusive re-equilibration of Nd and Pb in apatite. The inset shows the time required for a certain percent of re-equilibration to occur for each element of interest.

CHAPTER 6

CONCLUSIONS AND APPLICATIONS

The magnitude and ramifications of isotopic disequilibrium associated with partial melts may be extensive. Through use of a geochemical model, the potential offsets in ratios of partial melts were examined; disequilibrium was found to be most notable in the Pb and Nd isotopic systems due to the tendency of phases holding most of the budget for these elements remaining in the residual material. Apatite and zircon were the minerals of greatest interest in this study, but other accessory phases are also believed to be significant, particularly monazite for Nd. Mixing curves calculated in Section 5.1.2. illustrate that the assimilation of disequilibrium melts can change the isotopic signature of a basaltic magma body in ways currently attributed to whole rock assimilation. The implications of isotopic disequilibrium during anatexis on the process of migmatization were also examined through a diffusive re-equilibration model. Assuming that intra-crystalline diffusion in the residual minerals limits equilibration, this model suggests that for partial melts in still communication with their source each isotopic system may re-equilibrate at different timescales. If substantiated by experimental findings, the results of this study may prove to be useful tools in assessing the disequilibrium associated with anatexis and the geologic implications this may have.

LIST OF REFERENCES

Allègre, C.-J. and J.F. Minster (1978) Quantitative models of trace element behavior in magmatic processes. *Earth and Planetary Science Letters*. 38: 1-25.

Asimow, P.D. and M.S. Ghiorso (1998) Algorithmic modifications extending MELTS to calculate subsolidus phase relations. *American Mineralogist*. 83.9-10: 1127-1132.

Ayers, J.C., and E.B. Watson (1993) Apatite/fluid partitioning of rare-earth elements and strontium: Experimental results at 1.0 GPa and 1000°C and application to models of fluid-rock interaction. *Chemical Geology*. 110: 299-314.

Ayres, M., and N. Harris (1997) REE fractionation and Nd-isotope disequilibrium during crustal anatexis: constraints from Himalayan leucogranites. *Chemical Geology*. 139: 249-269.

Ayres, M., N. Harris, and D. Vance (1996) Possible constraints on anatectic melt residence times from accessory mineral dissolution rates: an example from Himalayan leucogranites. *Mineralogical Magazine*. 61: 29-36.

Baker, M.B., and E.M. Stolper (1994) Determining the composition of high-pressure mantle melts using diamond aggregates. *Geochimica et Cosmochimica Acta*. 58.13: 2811-2827.

Baker, J.A., M.F. Thirwall, and M.A. Menzies (1996) Sr-Nd-Pb isotopic and trace element evidence for crustal contamination of plume-derived flood basalts: Oligocene flood volcanism in western Yemen. *Geochimica et Cosmochimica Acta*. 60.14: 2559-2581.

Barbey, P., J.-M. Bertrand, S. Angoua, and D. Dautel (1989) Petrology and U/Pb geochronology of the Telohat migmatites. Aleksod, Central Hoggar, Algeria. *Contributions to Mineralogy and Petrolology*. 101: 207-219.

Bea, F. (1996) Residence of REE, Y, Th and U in granites and crustal protoliths; implications for the chemistry of crustal melts. Journal of Petrology. 37.3: 521-552.

Bea, F., and P. Montero (1999) Behavior of accessory phases and redistribution of Zr, REE, Y, Th, and U during metamorphism and partial melting of metapelites in the lower crust: An example from the Kinzigite Formation of Ivrea-Verbano, NW Italy. Geochimica et Cosmochimica Acta. 63.7/8: 1133-1153.

Bea, F., M.D. Pereira, and A. Stroh (1994) Mineral/leucosome trace-element partitioning in a peraluminous migmatite (a laser ablation-ICP-MS study). Chemical Geology. 117: 291-312.

Brady, J.B. (1995) Diffusion data for silicate minerals, glasses and liquids. In: Ahrens, T.J. Ed., Mineral Physics and Crystallography: A Handbook of Physical Constants. AGU, Washington DC: 269-290.

Bryce, J.G., and D.J. DePaolo (2004) Pb isotopic heterogeneity in basaltic phenocrysts. *Geochimica et Cosmochimica Acta*. 68.21: 4453–4468.

Carl, C., I. Wendt, and J.I. Wendt (1989) U/Pb whole-rock and mineral dating of the Falkenberg granite in northeast Bavaria. Earth and Planetary Science Letters. 94.3-4: 236-244.

Carslaw, H.S. and J.C. Jaeger. *Conduction of heat in solids.* 2nd Eds. New York: Clarendon Press, 1959.

Cherniak, D.J. (2000) Rare earth element diffusion in apatite. *Geochimica et Cosmochimica Acta*. 64: 3871-3885.

Chamberlain, K.R., and S.A. Bowring (2000) Apatite-feldspar U-Pb thermochronometer: a reliable, mid-range (~450°C), diffusion-controlled system. *Chemical Geology*. 72: 173-200.

Chamberlain, K.R., and S.A. Bowring (1990) Proterozoic geochronologic and isotopic boundary in NW Arizona. *Journal of Geology.* 98: 399-416.

Christensen, J.N. and D.J. DePaolo (1993) Time scales of large volume silicic magma systems: Sr isotopic systematics of phenocrysts and glass from the Bishop Tuff, Long Valley, California. *Contributions to Mineralogy and Petrolology*. 113: 100-114.

Conway, C.M., D.A. Gonzales, and K.R. Chamberlain (1989) Geologic map of Wabayuma Wilderness Area, Hualapai Mountains, Mohave County, AZ. *U.S. Geologic Survey Series Map*. MF-8973.

Conway, C.M., J.R. Hassemer, D.H. Knepper Jr., J.A. Pitkin, R.C. Jachens, and M.L. Chatman (1990) Mineral resources of the Wabayuma Peak Wilderness Study area, Mohave County, Arizona. *U.S. Geologic Survey Bulletin*. B1737.E.

Dahl, P.S., M.A. Hamilton, M.J. Jercinovic, M.P. Terry, M.L. Williams, and R. Frei (2005) Comparative isotopic and chemical geochronometry of monazite, with implications for U-Th-Pb dating by electron microprobe: An example from metamorphic rocks of the eastern Wyoming Craton (U.S.A.). *American Mineralogist*. 90: 619–638.

Davies, G.R., and S. Tommasini (2000) Isotopic disequilibrium during rapid crustal anatexis: implications for petrogenetic studies of magmatic processes. *Chemical Geology*. 162: 169–191.

DePaolo, D.J. (1981) Trace element and isotopic effects of combined wallrock assimilation and fractional crystallization. *Earth and Planetary Science Letters*. 53: 189-202.

DePaolo, D.J. and G.J. Wasserburg (1976) Nd isotopic variations and petrogenetic models. *Geophysical Research Letters*. 3: 249-252.

Dickin, A.P. *Radiogenic Isotope Geology*. Cambridge: Cambridge University Press, 2005.

Gardien, V., A.B. Thompson, D. Grujic, and P. Ulmer (1995) Experimental melting of biotite + plagioclase + quartz +/- muscovite assemblages and

implications for crustal melting. *Journal of Geophysical Research*. 100.B8: 15,581-15,591.

Green, T.H., and E.B. Watson (1982) Crystallization of apatite in natural magmas under high pressure, hydrous conditions, with particular reference to 'orogenic' rock series. *Contributions to Mineralogy and Petrology*. 79: 96-105.

Ghiorso, M.S. and R.O. Sack (1995) Chemical Mass-Transfer in Magmatic Processes IV. A Revised and Internally Consistent Thermodynamic Model for the Interpolation and Extrapolation of Liquid-Solid Equilibria in Magmatic Systems at Elevated-Temperatures and Pressures. *Contributions to Mineralogy and Petrology*. 119.2-3: 197-212.

Hammouda, T., M. Pichavant, and M. Chaussidon (1996) Isotopic equilibration during partial melting: an experimental test of the behaviour of Sr. *Earth and Planetary Science Letters*. 144: 109-121.

Harris, N., M. Ayres and J. Massey (1995) Geochemistry of granitic melts produced during the incongruent melting of muscovite: Implications for the extraction of Himalayan leucogranite magmas. *Journal of Geophysical Research*. 100: 15,767-15,778

Harris, N., D. Vance, and M. Ayres (2000) From sediment to granite: timescales of anatexis in the upper crust. *Chemical Geology*. 162: 155–167.

Harrison, T.M., and E.B. Watson (1984) The behavior of apatite during crustal anatexis: Equilibrium and kinetic considerations. *Geochimica et Cosmochimica Acta*. 48: 1467-1477.

Hirschmann, M. M., M. S. Ghiorso, L. E. Wasylenki, P. D. Asimow, and E. M. Stolper (1998) Calculation of Peridotite Partial Melting from Thermodynamic Models of Minerals and Melts. I. Review of Methods and Comparison with Experiments. Journal of Petrology. 39.6: 1091-1115.

Hogan, J.P. and A.K. Sinha (1991) The redistribution of lead isotopes during crustal anatexis: a model. *Geochimica et Cosmochimica Acta*. 35: 335-348.

Jacobsen, S.B. (1988) Isotopic constraints on crustal growth and recycling. *Earth and Planetary Science Letters*. 90: 315-329.

Jang, Y.D. and H.R. Naslund (2003) Major and trace element variation in ilmenite in the Skaergaard Intrusion: petrologic implications. *Chemical Geology*. 193: 109-125.

Karlstrom, K.E., and S.A. Bowring (1988) Early Proterozoic assembly of tectonostratigraphic terranes in southwestern North America. *Journal of Geology*. 96: 561-576.

Kent, A.J.R., J.A. Baker, and M. Wiedenbeck (2002) Contamination and melt aggregation processes in continental flood basalts: constraints from melt inclusions in Oligocene basalts from Yemen. *Earth and Planetary Science Letters*. 202: 577-594.

Knesel, K.M., and J.P. Davidson (2002) Insights into Collisional Magmatism from Isotopic Fingerprints of Melting Reactions. *Science*. 296: 2206-2208.

Knesel, K.M., and J.P. Davidson (1996) Isotopic disequilibrium during melting of granite and implications for crustal contamination of magmas. *Geology*. 24.3: 243-246.

Knesel, K.M., and J.P. Davidson (1999) Sr isotope systematics during melt generation by intrusion of basalt into continental crust. *Contributions to Mineralogy and Petrology*. 136: 285-295.

Küster, D., J. Liégeois, D. Matukov, S. Sergeev, and F. Lucassen (2008) Zircon geochronology and Sr, Nd, Pb isotope geochemistry of granitoids from Bayuda Desert and Sabaloka (Sudan): Evidence for a Bayudian event (920–900 Ma) preceding the Pan-African orogenic cycle (860–590 Ma) at the eastern boundary of the Saharan Metacraton. *Precambrian Research*. 164: 16-39.

Lanphere, M.A. (1968) Geochronology of the Yavapai Series of central Azrizona. *Canadian J. Earth Sciences*, 5, 757-762.

Le Breton, N. and A.B. Thompson (1988) Fluid-absent (dehydration) melting of biotite in metapelites in the early stages of crustal anatexis. *Contributions to Mineralogy and Petrolology*. 99: 226-237.

Li, X., X. Liang, M. Sun, Y. Liu, X. Tu (2000) Geochronology and geochemistry of single-grain zircons: Simultaneous in-situ analysis of U-Pb age and trace elements by LAM-ICP-MS. *European Journal of Mineralogy*. 12: 1015-1024.

Miller, C.F. and D.W. Mittlefehldt (1982) Depletion of LREE in felsic magmas. *Geology*. 10: 129-133.

Montel, J.M. (1986) Experimental determination of the solubility of Ce monazite in SiO_2-Al_2O_3-K_2O-Na_2O melts at 800°C, 2 kbar under H_2O saturated conditions. *Geology*. 14: 659-662.

Montel, J.-M. (1993) A model for monazite/melt equilibrium and application to the generation of granitic magmas. *Chemical Geology*. 110: 127-146.

Nelson, B.K., D.J. DePaolo (1985) Rapid production of continental crust 1.7 to 1.9 b.y. ago: Nd isotopic evidence from the basement of the North American mid-continent. *Geological Society of America Bulletin*. 96: 746-754.

Nold, J.L. (1984) Myrmekite in Belt Supergroup metasedimentary rocks-northeast border zone of the Idaho Batholith. *American Mineralogist*. 69: 1050-1052.

Patiño Douce, A.E. and J.S. Beard (1996) Effects of P, *f*(O2) and Mg/Fe ratio on dehydration melting of model metagraywackes. *Journal of Petrology*. 37.5: 999-1024.

Patiño Douce, A.E., and N. Harris (1998) Experimental Constraints on Himalayan Anatexis. *Journal of Petrology*. 39.4: 689–710.

Patiño Douce, A.E. and A.D. Johnston (1991) Phase equilibria and melt productivity in the pelitic system: implications for the origin of peraluminous granitoids and aluminous granulites. *Contributions to Mineralogy and Petrolology*. 107: 202-218.

Pichavant, M., J.-M. Montel, and L.R. Richard (1992) Apatite solubility in peraluminous liquids: Experimental data and an extension of the Harrison-Watson model. *Geochimica et Cosmochimica Acta*. 56: 3855-3861.

Poldervaart, A. and D. Eckelmann (1955) Growth phenomena in zircon of autochthonous granites. *Geologic Society of American Bulletin*. 66: 947-948.

Poller, U., J. Huth, P. Hoppe, and I.S. Williams (2001) Ree, U, Th, And Hf Distribution In Zircon From Western Carpathian Variscan Granitoids: A Combined Cathodoluminescence And Ion Microprobe Study. *American Journal of Science*. 301: 858-876.

Prince, C, J Kosler, D Vance, D Günther (2000) Comparison of laser ablation ICP-MS and isotope dilution REE analyses - implications for Sm–Nd garnet geochronology. *Chem. Geol.*, 168, 255-274.

Prinzhofer, A. and C.-J. Allègre (1985) Residual peridotites and the mechanisms of partial melting. *Earth and Planetary Science Letters*. 74: 251-265.

Prowatke, S., and S. Klemme (2006) Trace element partitioning between apatite and silicate melts. *Geochimica et Cosmochimica Acta*. 70: 4513–4527.

Rapp, R.P., and E.B. Watson (1986) Monazite solubility and dissolution kinetics: implications for the thorium and light rare earth chemistry of felsic magmas. *Contributions to Mineralogy and Petrology*. 94: 304-316.

Sawyer, E.W. (1991) Disequilibrium melting and the rate of melt-residuum separation during migmatization of mafic rocks from the Grenville Front, Quebec. *Journal of Petrology*. 32: 701-738.

Smith, P.M. and P.D. Asimow (2005) Adiabat_1ph: A new public front-end to the MELTS, pMELTS, and pHMELTS models. *Geochemistry Geophysics Geosystems*. 6.1.

Spera, F., and W. Bohrson (2001) Energy-Constrained Open-System Magmatic Processes I: General Model and Energy-Constrained Assimilation and

Fractional Crystallization (EC-AFC) Formulation. *Journal of Petrology*. 42.5: 999-1018.

Stensrud, H.L., and S. More (1980) Precambrian geology and massive sulfide environments of the West-Central Hualapai Mountains, Mohave County, Arizona: a preliminary report. In: Jenney, J.P. and C. Stone (Eds.), *Arizona Geological Society Digest, 12: Studies in Western Arizona*. 155-164.

Tommasini, S., and G.R. Davies (1997) Isotope disequilibrium during anatexis: a case study of contact melting, Sierra Nevada, California. *Earth and Planetary Science Letters*. 148: 273-285.

Thompson, A. B. (1982) Dehydration melting of pelitic rocks and the generation of H2O-undersaturated granitic liquids. *American Journal of Science*. 282: 1567-1595.

Vance, D., M. Meier, and F. Oberli (1998) The influence of high U-Th inclusions on the U-Th-Pb systematics of almandine-pyrope garnet: Results of a combined bulk dissolution, stepwise-leaching, and SEM study. *Geochimica et Cosmochimica Acta*. 60.21-22: 3527–3540.

Wasson, J.T. and G.W. Kallemeyn (1988) Compositions of Chondrites. *Philosophical Transactions of the Royal Society of London*. 325.1587: 535-544.

Waters, C.L., J.G. Bryce, and T. Furman (2004) Magmatic Processes under the East African Rift System: Insights from Melt Inclusions in Lavas of Turkana, Kenya. AGU, Spring 2004.

Watson, E.B. (1979) Zircon saturation in felsic liquids: experimental data and applications to trace element geochemistry. *Contributions to Mineralogy and Petrolology*. 70: 407-419.

Watson, E.B. (1988) The role of accessory minerals in granitoid geochemistry (abstract). *First Hutton Meeting on the Origin of Granites and Related Rocks*. Royal Society of Edinburgh. 19-20.

Watson, E.B., and C.J. Capobianco (1981) Phosphorus and the rare earth elements in felsic magmas: an assessment of the role of apatite. *Geochimica et Cosmochimica Acta*. 45: 2349-2358.

Watson, E.B. and T.M. Harrison (1983) Zircon saturation revisited: temperature and composition effects in a variety of crustal magma types. *Earth and Planetary Science Letters*. 64: 295-304.

Watson, E.B., and T.M. Harrison (1984) Accessory minerals and the geochemical evolution of crustal magmatic systems: a summary and prospectus of experimental approaches. *Physics of the Earth and Planetary Interiors*. 35: 19-30.

Watson, E.B., T.M. Harrison, and F.J. Ryerson (1985) Diffusion of Sm, Sr and Pb in fluorapatite. *Geochimica et Cosmochimica Acta,*. 49: 1813-1823.

Watson, E.B., E.P. Vicenzi, and R.P. Rapp (1989) Inclusion/host relations involving accessory minerals in high-grade metamorphic and anatectic rocks. Contributions to Mineralogy and Petrolology. 101: 220-231.

Watt, G.R., I.M. Burns, and G.A. Graham (1996) Chemical characteristics of migmatites: accessory phase distribution and evidence for fast melt segregation rates. *Contributions to Mineralogy and Petrolology*. 125: 100-111.

Watt, G.R., and S.L. Harley (1993) Accessory phase controls on the geochemistry of crustal melts and restites produced during water-undersaturated partial melting. *Contributions to Mineralogy and Petrology*. 114: 550-566.

Weaver, K.L., V.C. Bennett, D.J. DePaolo, and R. Mundil (2004) Disturbed Sr and Nd Isotope Systematics in Zircons With Concordant SHRIMP U-Pb Ages. *American Geophysical Union*, Fall 2004. Abstract #V51C-0592.

Weber, C. and P. Barbey (1987) Melting in migmatites; petrogenetic and experimental data (abstract). *First Hutton Meeting on the Origin of Granites and Related Rocks*. Royal Society of Edinburgh. 51.

White, A.J.R., I.S. Williams, and B.W. Chappell (1977) Geology of the Berridale 1:100,000 sheet. *Geologic Survey*. New South Wales, Department of Mines, Published No. 8625, 138.

Wimmenauer, W., and I. Bryhni (2007) A systematic nomenclature for metamorphic rocks: 6. Migmatites and related rocks. A proposal on behalf of the IUGS Subcommission on the Systematics of Metamorphic Rocks. *Recommendations*. Web version of 01.02.2007.

Zeng, L., P.D. Asimow, and J. Saleeby (2005(a)) Coupling of anatectic reactions and dissolution of accessory phases and the Sr and Nd isotope systematics of anatectic melts from a metasedimentary source. *Geochimica et Cosmochimica Acta*. 69.14: 3671–3682.

Zeng, L., J. Saleeby, and P.D. Asimow (2005(b)) Geochemical characteristics of crustal anatexis during the formation of migmatite at the Southern Sierra Nevada, California. *Contributions to Mineralogy and Petrology*. 150: 386–402.

Zeng, L., J. Saleeby, and P.D. Asimow (2005(c)) Nd isotope disequilibrium during crustal anatexis: A record from the Goat Ranch migmatite complex, southern Sierra Nevada batholith, California. *Geology*. 33.1: 53–56.

APPENDIX

Mineral	Th (ppm)	U (ppm)	Pb (ppm)	$^{206}Pb/^{204}Pb$	$^{207}Pb/^{206}Pb$	$^{208}Pb/^{204}Pb$	$^{208}Pb/^{206}Pb$
Quartz	0	0	0	0	0	0	0
Plagioclase	0.06	0.50	33.6	16.22	0.9451	36.38	2.24
Muscovite	0.03	0.16	0.44	23.68	0.6800	36.80	1.55
Biotite	0.01	0.20	1.32	19.14	0.8166	36.42	1.90
Garnet	3.91	1.05	0.11	219.1	0.1665	257.3	1.17
Sillimanite	0	0	0	0	0	0	0
K-Feldspar	7.33	2.05	30.0	15.90	0.9618	36.36	2.29
Apatite	21.8	16.1	9.20	116.7	0.1061	51.22	0.439
Monazite	62518	5482	2053	73.03	0.2909	227.2	3.11
Ilmenite	0.10	0.11	1.50	17.47	0.8845	36.79	2.11
Zircon	74.0	610	142	107.8	0.2307	39.63	0.368

Table A1. U, Th, and Pb concentrations and isotopic ratios (when t = 1.7 Ga) used in partial melt model. Values were amassed from the literature and represent compositions in these phases for granitic and pelitic rock sources (Bea 1996, Bea & Montero 1999, Bea *et al.* 1994, Carl et al 1989, Chamberlain & Bowring 2000, Dahl *et al.* 2005, Jang & Naslund 2003, Kuster et al 2007, Li *et al.* 2000, Poller *et al.* 2001, Vance *et al.* 1998). Isotopic ratios based on values for the Cherry Creek quartz diorite (part of the Ash Creek Block) in Arizona from Chamberlain and Bowring (2000), where $^{206}Pb/^{204}Pb_i$ = 15.898 and $^{208}Pb/^{204}Pb_i$ = 0.9618. Isotopic ratios then calculated using the appropriate age equation.

Mineral	Rb (ppm)	Sr (ppm)	$^{87}Sr/^{86}Sr$	Sm (ppm)	Nd (ppm)	$^{143}Nd/^{144}Nd$
Quartz	0	0	0	0	0	0
Plagioclase	1.70	490	0.7047	0.74	6.16	0.5114
Muscovite	242	119	0.8447	0.05	0.30	0.5117
Biotite	580	30.0	2.0378	0.05	0.29	0.5118
Garnet	1.01	2.49	0.7325	0.03	0.14	0.5121
Sillimanite	0	0	0	0	0	0
K-Feldspar	594	185	0.9259	0.10	0.73	0.5115
Apatite	0.33	263	0.7046	198	412	0.5139
Monazite	0	73.2	0.7045	18432	104361	0.5118
Ilmenite	0.29	0.64	0.7357	0.09	0.32	0.51124
Zircon	0.30	4.00	0.7097	3.1	5.9	0.51302

Table A2. Rb, Sr, Sm, and Nd concentrations and isotopic ratios (when t = 1.7 Ga) used in partial melt model. Values were amassed from the literature and represent compositions in these phases for granitic and pelitic rock sources (Ayres & Harris 1997, Bea & Montero 1999, Bea *et al.* 1994, Jang & Naslund 2003, Knesel & Davidson 1999, Li *et al.* 2000, Poller *et al.* 2001, Prince *et al.* 2000, Prowatke & Klemme 2006, Weaver et al 2004). Sr isotopic ratios based on values from the Ash Creek Block from Lanphere (1968), where $^{87}Sr/^{86}Sr_i$ = 0.7045. Nd ratios based on values from granite in northwestern Arizona reported in Nelson and DePaolo (1985), where $^{143}Nd/^{144}Nd_{now}$ = 0.512065 (normalized to $^{145}Nd/^{142}Nd$ = 0.63615 according to DePaolo & Wasserburg 1976). Isotopic ratios then calculated using the appropriate age equation

Rock Sample	Mineral (weight percent)						
	Qtz	Pl	Ms	Bt	Grt	Als	Ilm
Metapelite (MP)[1]	31.0%	4.0%	10.0%	30.0%	5.0%	19.0%	1.0%
Muscovite Schist (MS)[2]	43.0%	28.0%	22.0%	2.0%	5.0%		
Metagraywacke (MW)[3]	34.3%	26.5%		37.2%			2.0%

Table A3. Unmodified compositions used in partial melt studies. Qtz = quartz, Pl = plagioclase, Ms = muscovite, Bt = biotite, Grt = garnet, Als = aluminosilicate, Apt = apatite, Mnz = monazite, Ilm = ilmenite ([1]Patiño Douce & Johnston 1991, [2]Patiño Douce & Harris 1998, [3]Patiño Douce & Beard 1996).

T (°C)	P (kbar)	Qtz	Pl	Ms	Bt	Grt	Als	Ilm	Ox	Kfs	Melt	Name (this study)
Patiño Douce & Johnston (1991)												
825	10	18			33	4	25		1		18	MP
850	10	23			28	6	28		1		23	MP
875	10	22			25	11	21		1		21	MP
900	10	12			17	17	22		1		31	MP
925	10	5			20	19	19		1		35	MP
950	10	8			5	17	18		2		51	MP
975	10	8			1	14	16		3		58	MP
1000	10	1			0	17	18		3		60	MP
Patiño Douce & Harris (1998)												
775	6	42	25	15	3	5	1			1	8	MS
800	6	38	26	6	5	4	3			2	16	MS
820	6	35	21	0	4	4	5			5	25	MS
850	6	33	22	0	3	5	4			4	28	MS
900	6	32	22	0	1	9	4			0	32	MS
Patiño Douce & Beard (1996)												
850	10	22	11		20	19		1			26	MW
900	10	14	5		16	21		1			44	MW
925	10	9	0		0	33		2			56	MW
950	10	8	0		4	27		1			60	MW

Table A4. Experimental run products used for partial model (Ox = oxide, Kfs = potassium feldspar, rest of abbreviations follow those in Table A3, from Patiño Douce & Johnston 1991, Patiño Douce & Harris 1998, Patiño Douce & Beard 1996 as indicated).

T (°C)	P (kbar)	Na_2O	K_2O	MgO	Al_2O_3	SiO_2	FeO	Name (this study)
Patiño Douce & Johnston (1991)								
825	10	2.89	5.32	0.45	13.55	69.36	1.62	MP
850	10	2.24	5.69	0.41	14.25	70.86	1.7	MP
875	10	1.65	6.2	0.37	13.65	70.39	1.62	MP
900	10	1.29	6.06	0.41	13.46	71.54	1.61	MP
925	10	1.22	6.13	0.37	13.8	71.85	1.6	MP
950	10	1.1	6.86	0.33	13.46	73.66	1.65	MP
975	10	0.97	6.92	0.49	13.62	73.13	1.74	MP
1000	10	0.85	6.4	0.7	13.48	72.63	2.07	MP
Patiño Douce & Harris (1998)								
775	6	3.57	4.29	0.18	15.04	75.43	0.76	MS
800	6	3.22	4.91	0.21	15.86	74.09	1	MS
820	6	3.72	4.62	0.24	14.95	74.94	0.9	MS
850	6	3.85	4.99	0.24	15.01	74.3	0.94	MS
900	6	3.88	5.19	0.39	15.13	73.8	0.86	MS
Patiño Douce & Beard (1996)								
850	10	3.9	5.07	0.01	15.2	70.3	2.64	MW
900	10	2.91	5.09	0.01	15.3	71.2	2.45	MW
925	10	3.14	5.38	0.03	14.3	70.9	2.91	MW
950	10	3.79	5.61	0.02	14.8	70.2	2.9	MW

T(°C)	P(kbar)	CaO	MnO	TiO_2	F	P_2O_5	Total	Name (this study)
Patiño Douce & Johnston (1991)								
825	10	0.6	0.01	0.02	0	0.14	98.64	MP
850	10	0.39	0.05	0.13	0.1	0.05	100.19	MP
875	10	0.28	0.01	0.17	0.11	0.09	99.26	MP
900	10	0.23	0.03	0.21	0.08	0.1	98.48	MP
925	10	0.21	0.02	0.26	0.08	0.07	98.85	MP
950	10	0.13	0.05	0.37	0.08	0.04	101.29	MP
975	10	0.13	0.03	0.37	0.15	0.1	101.14	MP
1000	10	0.04	0.04	0.35	0.12	0.08	99.93	MP
Patiño Douce & Harris (1998)								
775	6	0.52	0.04	0.17			96.2	MS
800	6	0.49	0.05	0.15			96.79	MS
820	6	0.47	0.04	0.11			97.15	MS
850	6	0.46	0.06	0.15			97.86	MS
900	6	0.42	0.03	0.29			98.54	MS
Patiño Douce & Beard (1996)								
850	10	1.02	0.04	0.16	1.64		96.3	MW
900	10	1.07	0.03	0.16	1.78		97.20	MW
925	10	1.38	0.06	0.21	1.66		98.40	MW
950	10	1.08	0.03	0.18	1.43		98.20	MW

Table A5. Compositions of experimental melts used for partial model (from Patiño Douce & Johnston 1991, Patiño Douce & Harris 1998, Patiño Douce & Beard 1996 as indicated).

Rock Sample	Concentrations (ppm)						
	U	Th	Pb	Rb	Sr	Sm	Nd
MP *(0% zircon)*	0.19	0.26	1.82	196.87	41.21	0.55	1.40
MP *(0.01% zircon)*	0.25	0.27	1.84	196.81	41.21	0.55	1.40
MS	0.85	6.56	9.79	65.36	165.41	3.05	14.30
MW *(0% zircon)*	0.29	0.13	9.46	213.32	142.19	1.21	3.81
MW *(0.01% zircon)*	0.35	0.14	9.48	213.26	142.19	1.21	3.81

Table A6. Calculated trace element concentrations of whole rock compositions examined.

Rock Sample	% Melt	Concentrations (ppm)					
		Pb		Sr		Nd	
		Res.	Melt	Res.	Melt	Res.	Melt
MP							
(0% zircon)	1.82	0.00	41.21	0.00	1.40	0.00	1.82
	0.48	1.35	10.66	30.55	1.13	0.27	0.48
	0.41	1.41	9.21	32.00	1.12	0.28	0.41
	0.38	1.44	8.44	32.78	1.12	0.28	0.38
	0.28	1.54	6.19	35.03	1.10	0.30	0.28
	0.32	1.50	7.13	34.08	1.11	0.29	0.32
	0.14	1.69	2.59	38.62	1.07	0.33	0.14
	0.10	1.73	1.32	39.89	1.05	0.35	0.10
	0.09	1.74	1.09	40.12	1.05	0.35	0.09
(0.01% zircon)	1.84	0.00	41.21	0.00	1.40	0.00	1.84
	0.49	1.35	10.66	30.55	1.13	0.27	0.49
	0.43	1.41	9.21	32.00	1.12	0.28	0.43
	0.39	1.44	8.44	32.77	1.12	0.28	0.39
	0.30	1.54	6.19	35.03	1.10	0.30	0.30
	0.34	1.50	7.13	34.08	1.11	0.29	0.34
	0.15	1.69	2.59	38.62	1.07	0.33	0.15
	0.11	1.73	1.32	39.89	1.05	0.35	0.11
	0.10	1.74	1.09	40.12	1.05	0.35	0.10
MS							
	9.79	0.00	165.41	0.00	14.30	0.00	9.79
	9.06	0.73	144.55	20.87	14.10	0.20	9.06
	9.68	0.10	141.16	24.25	14.15	0.15	9.68
	8.86	0.92	114.77	50.64	13.84	0.46	8.86
	8.89	0.90	117.55	47.87	13.89	0.41	8.89
	7.67	2.12	109.64	55.77	13.86	0.44	7.67
MW							
(0% zircon)	9.46	0.00	142.19	0.00	3.81	0.00	9.46
	4.04	5.42	61.69	80.50	2.82	0.98	4.04
	1.98	7.49	31.14	111.05	2.44	1.37	1.98
	0.11	9.35	2.14	140.05	2.10	1.71	0.11
	0.14	9.32	3.18	139.01	2.09	1.71	0.14
(0.01% zircon)	9.48	0.00	142.19	0.00	3.81	0.00	9.48
	4.06	5.42	61.69	80.49	2.82	0.98	4.06
	1.99	7.49	31.14	111.05	2.44	1.37	1.99
	0.13	9.35	2.14	140.04	2.10	1.71	0.13
	0.16	9.32	3.18	139.00	2.09	1.71	0.16

Table A7. Calculated trace element concentrations of partial melts and residual material (Res).

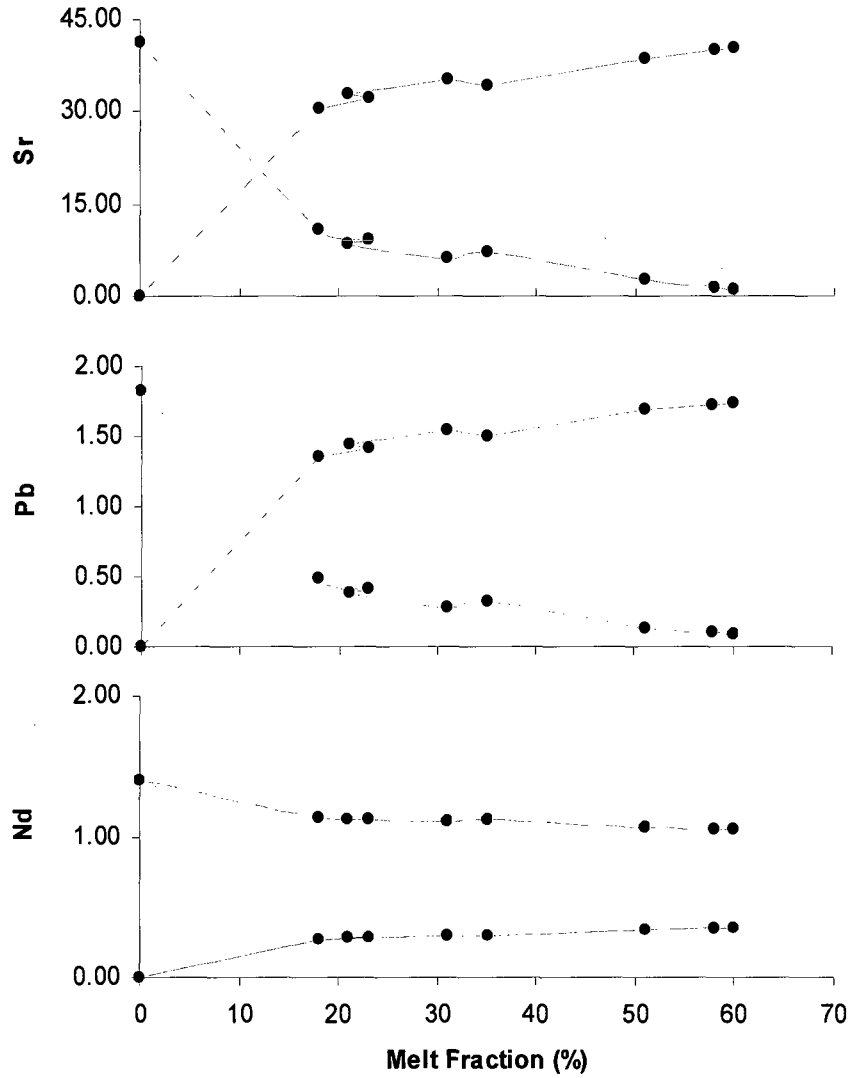

Fig. A1. Progression of trace element concentrations (in ppm) in source rock MP. Dashed lines indicate the concentration in the residual while solid lines represent those in the melt. The differences in concentrations between compositions with and without zircon were not significant enough to graph.

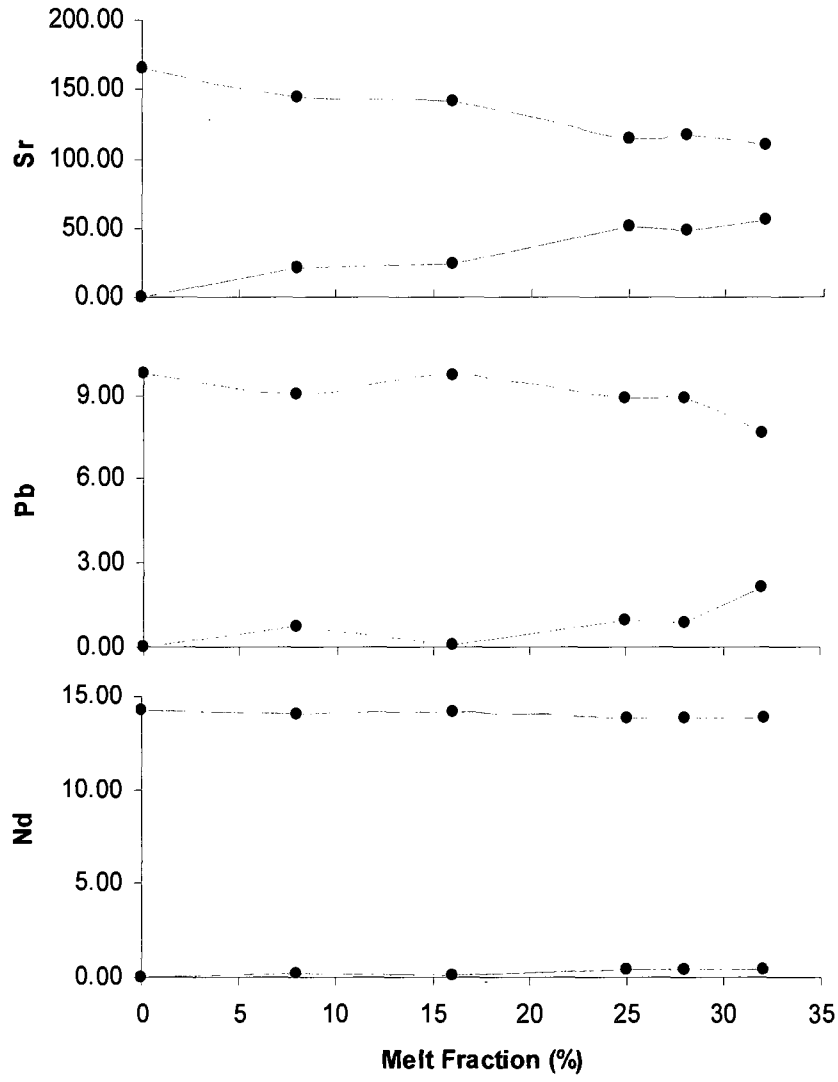

Fig. A2. Progression of trace element concentrations (in ppm) in source rock MS. Dashed lines indicate the concentration in the residual while solid lines represent those in the melt. As discussed in the text, the amount of Nd is substantially higher in this composition than the others due to monazite in the composition which remains in the residual throughout partial melting.

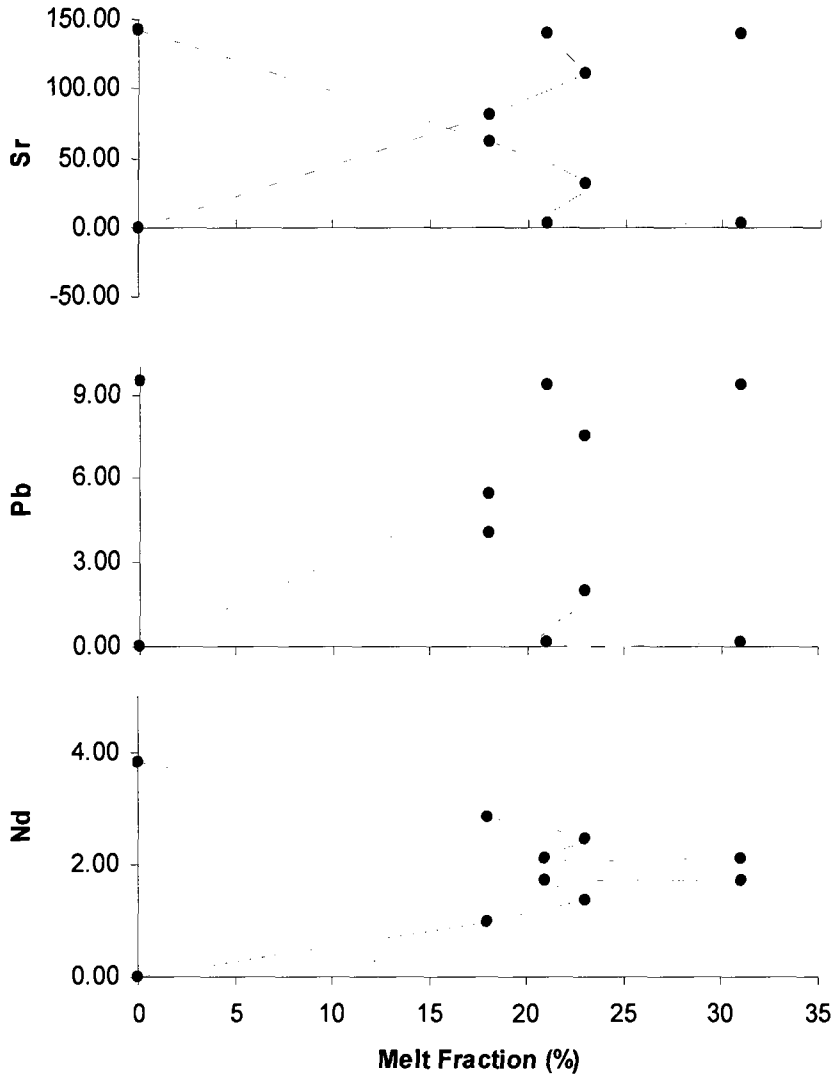

Fig. A3. Progression of trace element concentrations (in ppm) in source rock MW. Dashed lines indicate the concentration in the residual while solid lines represent those in the melt. The differences in concentrations between compositions with and without zircon were not significant enough to graph.

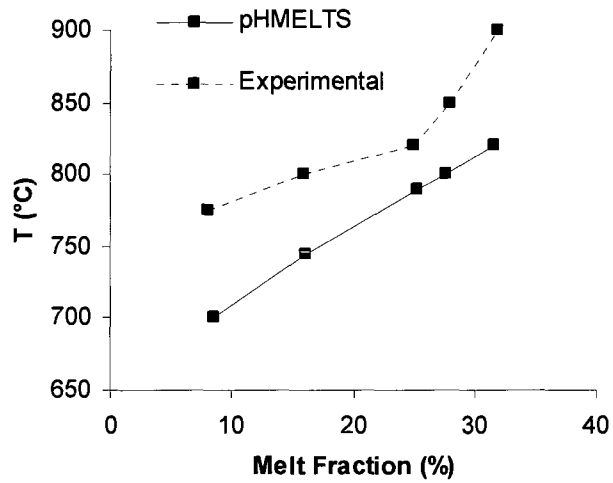

Fig. A4. Amount of melt produced from composition MS versus temperature. Experimentally determined by Patiño Douce and Harris (1998) and theoretically with pHMELTS.

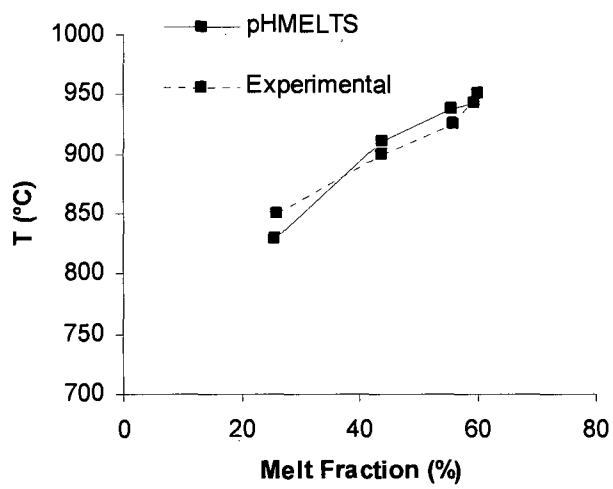

Fig. A5. Amount of melt produced from composition MW versus temperature. Experimentally determined by Patiño Douce and Beard (1996) and theoretically with pHMELTS.

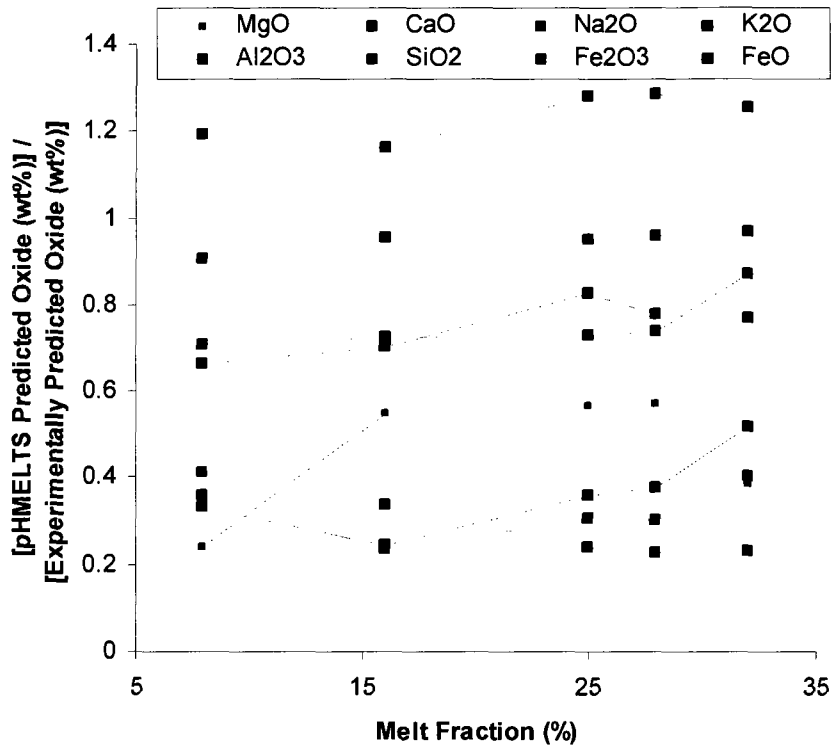

Fig. A6. Oxide composition of melts from MS as a ratio of the value predicted by pHMELTS and experiments (Patiño Douce & Harris 1998). Experimental FeO and Fe_2O_3 contents were calculated from FeO_{TOTAL} using MELTS (Ghiorso & Sack 1995). TiO_2 ratios ranged from ~1.3-6.4 and MnO ranged from ~7.6-35.

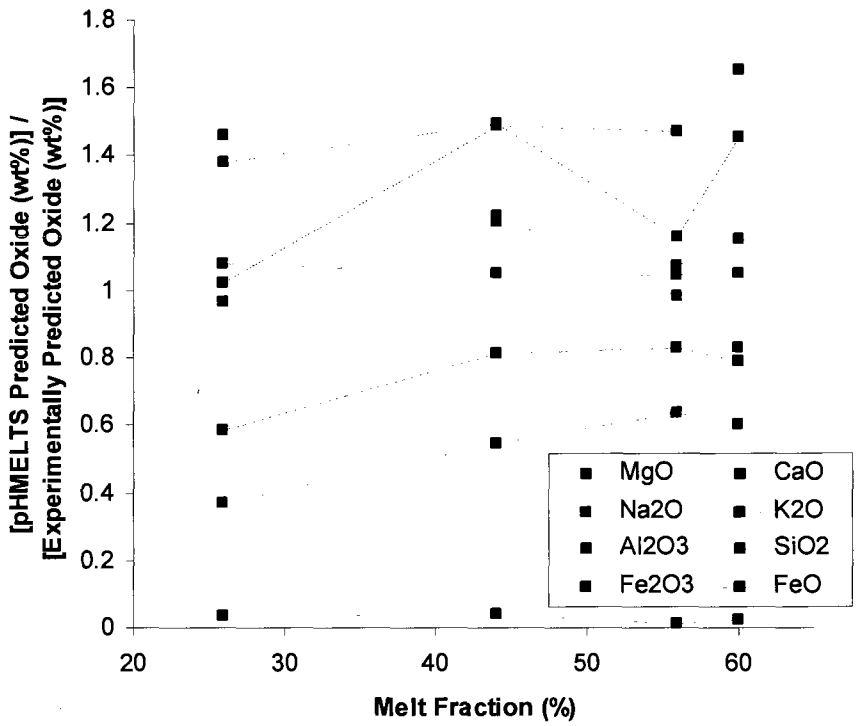

Fig. A7. Oxide composition of melts from MW as a ratio of the value predicted by pHMELTS and experiments (Patiño Douce & Beard 1996). Experimental FeO and Fe_2O_3 contents were calculated from FeO_{TOTAL} using MELTS (Ghiorso & Sack 1995). TiO_2 ratios ranged from ~1.9-5 and MnO ranged from ~11-34.

T (K)	M	D	Melt (wt%)	% of Zircon Entering Melt			
				0.1% Source Zircon	0.05% Source Zircon	0.03% Source Zircon	0.01% Source Zircon
1373	1.69	150.0	56	0.000015	0.000008	0.000005	0.000002
1423	1.84	94.56	67	0.000031	0.000016	0.000009	0.000003
1523	1.78	54.86	77	0.000075	0.000037	0.000022	0.000007
1773	1.70	17.79	99	0.000856	0.000428	0.000257	0.000086

Table A8. Values used to calculate the amount of zircon that will enter a felsic melt from a biotite granite with varied percentages of zircon (Knesel & Davidson 1999). T is the temperature in Kelvin, M is the cation ratio (Na + K + 2Ca)/(Al·Si), and D is the partition coefficient of zirconium between zircon and the melt under those conditions.

Oxide	Wt. %
SiO_2	69.94
TiO_2	0.49
Al_2O_3	14.04
FeO*	4.06
MnO	0.06
MgO	0.91
CaO	1.43
Na_2O	2.40
K_2O	5.15
P_2O_5	0.14
Sum	**98.60**
LOI (%)	0.89

Table A9. Unnormalized major element composition of Antler two-mica granite (sample AZ244 in Chamberlain & Bowring 1990, 2000). Total Fe is expressed as FeO*. LOI = lost on ignition, indicative of water content in the sample. Values determined through XRF analysis by the Washington State University GeoAnalytical Lab.

Element	Concentration (ppm)	Element	Concentration (ppm)
La	61.56	**Ba**	657
Ce	117.19	**Th**	23.67
Pr	15.20	**Nb**	24.43
Nd	55.54	**Y**	40.53
Sm	10.41	**Hf**	4.28
Eu	0.95	**Ta**	1.73
Gd	8.47	**U**	1.52
Tb	1.34	**Pb**	31.05
Dy	7.93	**Rb**	318.8
Ho	1.53	**Cs**	8.08
Er	4.10	**Sr**	105
Tm	0.59	**Sc**	9.0
Yb	3.50	**Zr**	158
Lu	0.52		

Table A10. Trace element concentrations of Antler two-mica granite (sample AZ244 in Chamberlain & Bowring 1990, 2000). Analyzed by ICP-MS by the Washington State University GeoAnalytical Lab.